Beyond Ornithine Metabolism in Gyrate Atrophy: Tissue-Specific Proteomic Insights into Neonatal and Adult OAT Deficiency

Artjola Puja[1,2], Rong Xu[1,2], Mark Eminhizer[1,2], Tuan Ngo[1,2], Ying Zhang[1,2], Qingyan Wang[1,2], Meghashri Saravanan[1, 2], Jianhai Du[1,2]*

[1]Department of Ophthalmology and Visual Sciences, West Virginia University, Morgantown, WV 26506

[2]Department of Biochemistry and Molecular Medicine, West Virginia University, Morgantown, WV 26506

*Corresponding Authors: Jianhai Du, One Medical Center Dr, PO Box 9193, WVU Eye Institute, Morgantown, WV 26505

Phone: (304) 293-9346

Fax: (304)-598-6928

Email: jianhai.du@hsc.wvu.edu.

Keywords: ornithine aminotransferase; ornithine; gyrate atrophy; retina; retinal pigment epithelium; neonatal metabolism; retinal degeneration; proteomics

ABSTRACT

Ornithine aminotransferase (OAT) links the urea and TCA cycles by interconverting ornithine to pyrroline-5-carboxylate. Despite its abundance in the liver, OAT mutations primarily cause gyrate atrophy (GA) and blindness. Paradoxically, adult GA patients have hyperornithinemia that is managed by arginine-restricted diet, while neonates experience hypoornithinemia and require arginine supplementation to prevent mortality in animal models. To understand this biochemical paradox, we performed a comprehensive proteomic analysis of the liver, retina, and retinal pigment epithelium and choroid (RPE/Cho) in neonatal and adult *Oat*^{rhg} mice, a whole-body OAT-deficient model. We found that the number of significantly altered proteins ranged from 5 to 254 across tissues and ages, with minimal changes in the adult retina and greatest changes in the adult RPE/Cho. OAT was the only protein consistently downregulated across all tissues. Neonatal liver proteome was more extensively altered than the adult liver proteome, primarily impacting metabolic pathways, including fatty acid oxidation, detoxification, cholesterol synthesis, and the urea cycle. In contrast, the adult liver showed changes mainly in detoxification and chromosome remodeling. Similarly, the neonatal retina was far more sensitive to OAT deficiency, with alterations not only in metabolism but also in visual transduction, ion and small molecule transport proteins. The RPE/Cho displayed the most pronounced changes in both age groups. In adults, several mitochondrial and signaling proteins were downregulated, while proteins in lipid metabolism, cytoskeleton, and extracellular matrix (ECM) were upregulated. In neonates, the alterations were enriched in chromatin organization, ECM, and vesicle transport. In summary, our findings reveal that OAT is crucial for maintaining age- and tissue-specific proteome homeostasis, with its deficiency leading to alterations in mitochondrial, metabolic processes, and signaling pathways that extend far beyond its canonical role in ornithine metabolism.

INTRODUCTION

Ornithine aminotransferase (OAT) is a mitochondrial enzyme that catalyzes the reversible transamination of ornithine, a urea cycle intermediate, and α-ketoglutarate to generate pyrroline-5-carboxylate and glutamate, precursors for proline synthesis. As glutamate and proline feed into tricarboxylic acid (TCA) cycle intermediates, the OAT reaction serves as a crucial link between the urea and TCA cycle. Mutations in the *OAT* gene cause gyrate atrophy (GA), a rare

autosomal recessive blinding disorder characterized by markedly elevated systemic ornithine levels[1–3]. Vision impairment often appears in late childhood, with myopia and night blindness, followed by cataracts and visual field constriction, ultimately leading to vision loss by mid-adulthood[4,5]. Beyond the eye, patients with GA can also present with neurological and muscular symptoms, while affected neonates may have hyperammonemia, lethargy, vomiting, and encephalopathy, which mimic primary urea cycle disorders[6,7].

A biochemical paradox of OAT deficiency is the age-dependent inversion of plasma ornithine and arginine levels. Human infants with GA often lack visual symptoms, but present with low systemic ornithine levels and hyperammonemia[6]. Germline deletion of the *Oat* gene in mice causes hypoornithinemia and neonatal mortality, a phenotype that can be rescued by supplementing arginine, the immediate precursor of ornithine[8]. Arginine is an essential nutrient in early life, sustaining the urea cycle, protein synthesis, and growth[9,10]. After weaning, however, both mice and human patients develop hyperornithinemia[8]. This biochemical paradox presents a therapeutic contradiction in GA: arginine restriction is used to lower ornithine in older patients and slow degeneration, whereas arginine supplementation is vital for neonatal survival in mice[3,4,11]. Moreover, clinical outcomes in GA do not always correlate with systemic ornithine levels, pointing to more complex, tissue-specific disease mechanisms[12,13].

The liver has the highest expression of OAT, making it a critical organ in GA pathophysiology[14,15]. Liver-directed gene therapy partially rescues the retinal phenotype and reduces systemic ornithine in the disease mouse model[15]. The retinal pigment epithelium (RPE), a monolayer of cells positioned between the neural retina and choroidal circulation, is particularly vulnerable to early damage, which often precedes retinal degeneration in both animal models and human patients[2,16]. Restoration of OAT expression in the liver and retina of *Oat*^{rhg} mice reduces systemic ornithine, while improving retinal function and morphology compared to either tissue alone[17], demonstrating the importance of both systemic and local OAT function.

Despite the profound systemic effects observed in GA patients, the tissue-specific effects of OAT deficiency, particularly prior to retinal degeneration, remain poorly characterized. To investigate these effects, we used the *Oat*^{rhg} mouse model (*Oat*$^{G353A/G353A}$), which recapitulates the key age-dependent biochemical and ocular features of GA (**Figure 1B, C**)[18]. We performed a comprehensive, quantitative proteomic analysis of the liver, RPE/Choroid (RPE/Cho), and retina from both neonates and adults. We found that OAT deficiency triggers distinct age- and

tissue-dependent proteomic changes, affecting not only amino acids, but also lipid metabolism, detoxification, nuclear processes, and cytoskeletal integrity. This study presents a comprehensive proteomic atlas of OAT deficiency, revealing OAT as a pivotal regulator of diverse metabolic pathways, chromatin dynamics, and signaling pathways in a tissue- and age-specific context. These findings provide critical mechanistic insights into the longstanding biochemical enigma of OAT-related metabolic dysregulation.

EXPERIMENTAL PROCEDURES

Animals

All animal procedures were conducted in accordance with National Institutes of Health guidelines and were approved by the Institutional Animal Care and Use Committee (IACUC) of West Virginia University. *Oat* homozygous mutants (*Oat*^{rhg}*)* mice were obtained from the Jackson Laboratory and bred onto a C57BL/6J background for more than three generations before use in experiments. Heterozygous *Oat*$^{rhg+/-}$ mice retain OAT activity comparable to wild-type controls[18]. To increase colony yield, homozygous and heterozygous mice were intercrossed. Neonates (postnatal day 11) and adults (postnatal day 112) of both genotypes were used for experiments. Genotyping was performed by Transnetyx, Inc. (Cordova, TN; see **Table S1**). Due to the lethal phenotype caused by OAT deficiency in *Oat*^{rhg} neonates, we administered daily intraperitoneal injections of arginine (1 µL/g body weight of a 500 mM solution, pH 7) from P8 to P20. The solution was prepared from 0.33 M arginine hydrochloride and 0.17 M arginine base (see **Table S1**). Additionally, because of their delayed development, *Oat*^{rhg} mutant pups were kept with their mothers for approximately 40 days before weaning, until their body size could support independent survival. In this study, the P11 neonates did not receive arginine supplementation, while the adult mice received it during their neonatal period as described. All animals were housed under standard conditions with ad libitum access to standard chow and water.

Tissue collection and sample preparation

Samples were collected around noon from neonatal (P11) and adult (P112) *Oat*^{rhg} and littermate *Oat*$^{rhg+/-}$ control mice of both sexes. Prior to tissue collection, all animals were transferred to a procedure room and acclimated for one hour. Mice were euthanized via cervical dislocation. Their eyes were immediately enucleated, and the surrounding muscle and fat were carefully removed. The neural retina and RPE/Cho were then isolated in cold HBSS by dissecting the

anterior segments as previously described[19]. Because the RPE is difficult to separate from its tightly bound choroid, and the choroid plays an important role in RPE function, we analyzed the RPE/choroid complex (RPE/Cho) as in our previous studies[20]. A small section from the right lobe of the liver was excised and rapidly rinsed in cold PBS. All collected tissues were flash-frozen in liquid nitrogen. Proteins from the retina, RPE/Cho, and liver were extracted using radioimmunoprecipitation assay (RIPA) buffer with protease and phosphatase inhibitors (5 mg/mL). The tissue lysates were centrifuged at 12,000 rpm for 15 minutes at 4°C, and the supernatant was used to measure protein concentration by BCA assay. The quantitative proteomic analysis was performed by IDeA National Resource for Quantitative Proteomics (Little Rock, Arkansas).

Quantitative proteomics

Total protein from each sample was reduced, alkylated, and purified by chloroform/methanol extraction prior to digestion with sequencing grade modified porcine trypsin (Promega). Tryptic peptides were then separated by reverse phase XSelect CSH C18 2.5 um resin (Waters) on an in-line 150 x 0.075 mm column using an UltiMate 3000 RSLCnano system (Thermo). Peptides were eluted using a 60 min gradient from 98:2 to 65:35 buffer A:B ratio (Buffer A contains 0.1% formic acid, 0.5% acetonitrile. Buffer B contains 0.1% formic acid, 99.9% acetonitrile). Eluted peptides were ionized by electrospray (2.2 kV) followed by mass spectrometric analysis on an Orbitrap Exploris 480 mass spectrometer (Thermo). To assemble a chromatogram library, six gas-phase fractions were acquired on the Orbitrap Exploris with 4 m/z DIA spectra (4 m/z precursor isolation windows at 30,000 resolution, normalized AGC target 100%, maximum inject time 66 ms) using a staggered window pattern from narrow mass ranges using optimized window placements. Precursor spectra were acquired after each DIA duty cycle, spanning the m/z range of the gas-phase fraction (i.e. 496-602 m/z, 60,000 resolution, normalized AGC target 100%, maximum injection time 50 ms). For wide-window acquisitions, the Orbitrap Exploris was configured to acquire a precursor scan (385-1015 m/z, 60,000 resolution, normalized AGC target 100%, maximum injection time 50 ms) followed by 50x 12 m/z DIA spectra (12 m/z precursor isolation windows at 15,000 resolution, normalized AGC target 100%, maximum injection time 33 ms) using a staggered window pattern with optimized window placements. Precursor spectra were acquired after each DIA duty cycle.

Proteomics data analysis

Following data acquisition, data were searched using an empirically corrected library against the

UniProt Mus musculus database (Proteome ID:UP000000589, 2nd version of 2023) and a quantitative analysis was performed to obtain a comprehensive proteomic profile. Proteins were identified and quantified using EncyclopeDIA[21] and visualized with Scaffold DIA using 1% false discovery thresholds at both the protein and peptide level. Protein MS2 exclusive intensity values were assessed for quality using ProteiNorm[22]. The data was normalized using Cyclic Loess[23] and analyzed using proteoDA to perform statistical analysis using Linear Models for Microarray Data (limma) with empirical Bayes (eBayes) smoothing to the standard errors[24,25]. Proteins with an FDR adjusted p-value < 0.05 and a fold change (FC) > 2 were considered significant.

Proteomic pathway analysis

Pathway enrichment and functional annotation of differentially expressed proteins were performed using STRING (v12.0)[26] and DAVID[27]. Differential expression was defined by a Log_2 fold change ≥ ±1 and a p-value < 0.05. Protein-protein interaction networks were generated using STRING, and pathway analysis results from DAVID were visualized with GraphPad Prism (v9.5.1; GraphPad Software, Inc). Venn diagrams were generated using InteractiVenn[28] to visualize the overlap of proteins across different sample groups. Metabolic proteins were annotated by integrating the list of significantly altered proteins from proteomic analysis with a previously published metabolic gene set[29]. This list was subsequently refined through manual curation using UniProt and targeted NCBI/PubMed searches. For each protein, NCBI was queried using combinations of relevant keywords (e.g., *"[protein name] AND (eye OR vision OR retina OR RPE OR liver OR metabolism OR disease)"*) to identify studies linking the protein to specific tissues or metabolic functions.

Liquid chromatography–mass spectrometry (LC-MS)

Plasma and tissue ornithine were measured by LC-MS. Mouse retina, RPE/Cho, and liver (small piece from the same lobe) were quickly harvested, weighed, and snap-frozen in liquid nitrogen. Metabolites from tissues were extracted by homogenization in 80% cold methanol, as previously described[20]. Samples were centrifuged at 13,000 rpm for 15 min at 4 °C, and the supernatants from the retina, RPE/Cho, and liver, were used for ornithine analysis. Ornithine levels were analyzed by LC-MS with a Shimadzu LC Nexera system coupled to an AB Sciex QTRAP 5500 mass spectrometer (AB Sciex, Toronto, ON, Canada) using multiple monitoring reaction method as described previously[29,30]. The ornithine peak was identified and quantified using MultiQuant Software Version 3.0 for the retina, RPE/Cho, and liver samples.

Immunoblot

Immunoblots were performed as previously described[31]. Briefly, tissue samples containing 20 μg protein were separated in Mini-PROTEAN TGX precast gels, transferred onto 0.22 μm nitrocellulose membranes, and blocked with 5% non-fat milk in 1× Tris-Buffered Saline with 0.1% Tween-20 (TBST). Membranes were incubated overnight at 4°C with primary antibodies (1:1000 dilution; see **Table S1**) and then in horseradish peroxidase (HRP)-conjugated secondary antibodies (1:2000) for 1 hour, followed by visualization by chemiluminescence.

Statistics

Ornithine ion abundances in *Oat*^{rhg} mice were divided by those from *Oat*$^{rhg+/-}$ mice to calculate fold changes (FC). Data were graphed using GraphPad Prism (v9.5.1). Statistical significance was determined using multiple unpaired t-tests with Bonferroni correction method, with $p < 0.05$ considered significant. All data are presented as the mean ± SD.

RESULTS

Loss of OAT causes opposite effects on plasma and tissue ornithine in *Oat*^{rhg} mice

To understand the early changes leading to neonatal mortality and retinal degeneration in adults with OAT deficiency, we assessed visual function, protein expression, and ornithine levels in neonatal (P11) and adult (P112) *Oat*^{rhg} and *Oat*$^{rgh+/-}$ control littermates. Electroretinogram (ERG) assessments confirmed that visual function was normal in *Oat*^{rhg} adult mice, indicating the absence of retinal degeneration at this stage (**Figure S2**). Although loss of OAT enzymatic activity in *Oat*^{rhg} mice is established[18], it was unknown whether these mice lack OAT protein expression in ocular tissues. Immunoblot analyses demonstrated a complete lack of OAT protein in both the retina and RPE/Cho, confirming its absence in mutant mice (**Figure 1D, E, S1**). Consistent with previous reports, plasma ornithine levels were markedly reduced in neonates, but were significantly elevated in adult *Oat*^{rhg} mice[7,8,32] (**Figure 1F**). Notably, ornithine concentrations in neonatal tissues were considerably decreased, whereas in the adult liver, retina, and RPE/Cho, levels were dramatically increased, exceeding those of controls by over 20-fold (**Figure 1G**). These findings suggest that OAT exerts distinct, age-specific functions within these tissues.

OAT deficiency alters liver proteome in mutiple pathways beyond ornithine metabolism

To determine the molecular changes underlying the OAT deficiency in the liver, we conducted a quantitative proteomic profiling of adult *Oat*^{rhg} and *Oat*$^{rhg+/-}$ mice. The proteomics analysis

identified 62 differentially expressed (DE) proteins in adult *Oat*^{rhg} mouse liver compared to controls (**Figure 2A**). As expected, OAT was the most significantly changed protein with approximately 9-fold decrease. Functional categorization of these DE proteins revealed a significant enrichment in metabolism (34%), followed by transcription (18%), cytoskeleton (13%), immunity (11%), and signal transduction (10%) (**Figure 2B**). Subcellular localization analysis showed that these proteins were predominantly associated with the cytoplasm, endoplasmic reticulum (ER), nucleus, and membranes, while mitochondrial and lysosomal proteins were less affected (**Figure 2C**). Gene ontology (GO) analysis revealed that the top four enriched pathways in the OAT-deficient adult liver were nucleosome assembly, as well as steroid, alcohol, and xenobiotic metabolism (**Figure 2D**).

To further assess the proteomic changes in these pathways, we examined the changes in expression of specific proteins contributing to each of these main categories (**Figure 2E**). The analysis revealed substantial disruption of the Phase I and II detoxification pathways, involving cytochrome P450 enzymes (CP341, CP17A, CP3AG, CP341) and sulfotransferases (ST2A1, ST2A5, ST2A8, ST3A1), which are critical for the metabolism of drugs, steroids, bile acids, and fatty acids. Flavin-contain monooxygenase 3 (FMO3), a key hepatic monooxygenase, was also markedly reduced, potentially impairing the overall detoxification capacity of liver in *Oat*^{rhg} mice. Surprisingly, several histone H2B variants (H2B1F, H2B1M, H2B1C) and demethylases (KDM3B) were upregulated, suggesting chromatin remodeling and transcriptional alterations. Significant alterations were also found in cytoskeletal proteins, including MYH7B, DESP, MAP1B, CPLX4, and TBA1C, pointing to potential remodeling of cell structure and intracellular transport. Furthermore, we identified significant upregulation of inflammatory and immune-related proteins in the livers of *Oat*^{rhg} mice, including histocompatibility class II proteins (O19441, Q8HWB2, HA2K) (**Figure 2E**). Taken together, these results illustrate that OAT deficiency in the adult liver extends beyond amino acid transamination, potentially impacting diverse pathways including lipid metabolism, detoxification, transcriptional regulation, cytoskeletal integrity, and immune responses (**Figure 2F**).

OAT deficiency alters metabolism and detoxification proteins in the neonatal liver

The effects of OAT deficiency on the neonatal hepatic proteome were more extensive than in adults, with a total of 87 significantly changed proteins, including 47 downregulated and 40 upregulated (**Figure 3A**). Detoxification enzymes (EST1, EST3A, CP2CT, CP254) and proteins involved in amino acid metabolism (GSTP3, CAH3) were among the most significantly altered,

while OAT expression was reduced more than 2-fold. Notably, iron storage proteins, such as FRIL1 and FRIH were upregulated in neonates (**Figure 3A**), suggesting dysregulated liver iron homeostasis. Functional annotation highlighted metabolism as the dominant category with 79% of changed proteins, followed by signaling (7%), and immunity (6%) (**Figures 3B**). Subcellular location analysis showed that the DE proteins were predominantly found in the cytoplasm and ER (**Figure 3C**). Pathway enrichment grouped these changes into three clusters, and identified disruption in fatty acid metabolism, detoxification, thyroid hormone metabolism, and immune responses **(Figure 3D**). STRING analysis of these clusters showed enrichment of cytochrome P450 enzymes involved in arachidonic and linoleic acid metabolism (**Figure 3E**). Phase I detoxification enzymes were broadly downregulated, whereas phase II enzymes showed mixed regulation (**Figure 3F**).

Beyond detoxification, OAT deficiency in neonates shifted lipid metabolism toward increased cholesterol biosynthesis (ERG7, FDFT, and CP51A) and decreased fatty acid breakdown (OCTC, HAOX2, LICH). Additionally, metabolic pathways including glucose metabolism (PCKGC, ALDOC, KPYR, PHKG2, INO1), nitrogen metabolism (AATC, ASSY), glutathione metabolism (GSTP3, GSTA3), and carbonic anhydrases (CAH3, CAH5A) were also significantly affected (**Figure 3F**), suggesting a broad impact of OAT loss on the neonatal liver metabolism. Importantly, several immune modulators including STAT1, IL1RA, TGTP1, TGTP2, IGTP, and MVP were significantly upregulated (**Figure 3G**). When comparing neonatal to adult liver proteomics, we found four consistently altered proteins: OAT, as well as CP3AG, ST2A5, and ST2A1, which are associated with detoxification, indicating that this is a common susceptibility linked to OAT deficiency across developmental stages (**Figure S3**). Together, these findings establish OAT as a critical regulator of hepatic metabolism and demonstrate that its deficiency in neonates rewires lipid, glucose, nitrogen, and detoxification pathways, which likely underlies the early lethality observed in *Oat*^{rhg} mice (**Figure 3H**).

OAT loss induces widespread changes in the neonatal retinal proteome with minimal effects in adults

Proteomic analysis showed striking age-dependent differences in *Oat*^{rhg} retinas. Only 5 DE proteins were identified in adult retinas, with 3 downregulated, including OAT, and 2 upregulated (**Figure 4A**). In contrast, the neonatal retina contained 87 DE proteins, with 43 downregulated and 44 upregulated (**Figure 4B**). OAT was the only protein consistently downregulated across both age groups (**Figures 4C–D**). In adults, the DE proteins were

primarily associated with cytoskeletal regulation (LIMA1, ROCK1) and synapse modulation (CAD13). To investigate which retinal cell types might be most affected by OAT deficiency, proteins significantly altered in our dataset were mapped using previously published single-cell transcriptomic data from normal mouse retina[33]. The analysis showed that CAD13, OAT, and LIMA1 are normally enriched in horizontal cells, amacrine cells, and Müller glia, suggesting selective vulnerability of interneuron and glial populations in OAT deficiency (**Figure 4E**).

In neonatal retinal proteome, DE proteins were predominantly enriched in metabolism (33%), transcriptional regulation (22%), and signal transduction (22%) (**Figure 4F**), with subcellular localization distributed across membrane, nuclear, and cytoplasmic compartments (**Figure S4**). GO analysis highlighted dysregulated pathways involved in lipid synthesis, ion transport, sensory transduction, cellular differentiation, and transcriptional processes (**Figure 4G**). However, manual classification of enriched proteins suggested that OAT deficiency mainly impacts pathways involved in amino acid, lipid, and small molecule transport (**Figure 4H**). Specifically, enzymes related to proline synthesis (P5CR1), glutamine metabolism (GLNA), as well as cholesterol and fatty acid metabolism (FDFT, OSB10, DECT2, DEGS1) were significantly altered. In addition, transporters for glutamate (VGLU1), urea (UT1), and the mitochondrial ADP/ATP exchanger (ADT4) proteins were decreased, indicating compromised nutrient transport and metabolite exchange. Strikingly, the expression of key phototransduction proteins was also suppressed, including PDE6A, PDE6B, and opsins, in the neonatal *Oat*^{rhg} retina (**Figure 4K**). Conversely, several transcriptional regulators, including TLE4, LRRF1, JARD2, and DNLI1 were upregulated, many of which are associated with retinal development and the regulation of Wnt signaling pathway[34–36] (**Figures 4B, 4L; S5**). Supporting these findings, phenotype ontology analysis (Monarch) associated these proteomic alterations with defective photoreceptor outer segment (POS) structure and retinal dysfunction (**Figure S6**). Collectively, we have found OAT deficiency has a minimal impact on the retinal proteome in adults, but it extensively alters proteins in metabolic, transcriptional, and phototransduction pathways, suggesting neonatal retina is highly sensentive to metabolic stressors.

OAT deficiency induces metabolic and structural proteome changes in adult RPE/Cho

Among the adult tissues, the RPE/Cho showed the most profound proteomic changes, with 254 DE proteins identified (155 downregulated and 99 upregulated; **Figure 5A**). Alterations spanned metabolism (38%), cytoskeleton (15%), and signaling pathways (13%), with substantial upregulation of crystallin proteins (CRYAA, CRBB2) (**Figure 5A, B**). GO analysis revealed that mRNA processing, ER–Golgi trafficking, and mitochondrial bioenergetics were diminished. In

contrast, pathways related to lipid and fatty acid metabolism, as well as cellular transport processes were upregulated (**Figure 5C**). Most of these DE proteins were localized in the cytoplasm, mitochondria, and ER compartments (**Figure 5D**). Given the essential role of RPE metabolism in supporting retinal health[37,38], we further analyzed the enriched metabolic proteins and their associated processes. Key proteins regulating redox balance (SELT, AOXB, RT4I1, GSTP1), amino acid metabolism (P5CR2, LPP60, KCRS, GPX3), and sugar metabolism (MPI, PGAM2, PFKFB1, AMY1) were significantly downregulated (**Table S8**). Additionally, mitochondrial transporters (TOM22, MPC1), electron transport chain (ETC) components (CX7A1, COX2, NDUS8, NDUF4), amino acid (P5CR2, KCRS), and fatty acid metabolism enzymes (CPT1B, ABHDB, ACPM) were also reduced. Collectively, these changes indicate compromised mitochondrial function, bioenergetics, and nutrient metabolism in the RPE/Cho of *Oat*^{rhg} mice (**Figure 5E**).

In contrast, proteins such as the ε-subunit of ATP synthase (ATP5E), peroxisomal fatty acid metabolism enzyme OCTC, and several ER-associated lipid enzymes (AAAD, DHB2, SPTC2, LMF1) were upregulated. Ion channels including TPC1, KCJ13, CLA4A, and VATB1 also showed increased expression (**Figure 5E**). Interestingly, the mRNA processing pathway was prominently affected, with the downregulation of several ribosomal subunits (RL21, RL32, RL34, RS21) and the mitochondrial ribosomal protein RT35 (**Figure 5F**) suggesting the translational capacity in the RPE/Cho may be impaired. Additionally, crystallin family proteins (CRYAA, CRBB1, CRBB2) were upregulated, potentially reflecting cellular stress response, consistent with previous reports[39,40]. Pathway mapping of the altered proteins indicated enhanced mammalian target of rapamycin (mTOR) signaling and reduced mitogen-activated protein kinase (MAPK) signaling (**Figure 5F**). Significant alterations were also observed in cytoskeletal, intermediate filament, and ECM proteins, suggesting substantial intracellular and tissue remodeling. For example, myosin proteins were downregulated, while keratins and several ECM components (CILP2, COL1A2, CO6A6, KERA) were upregulated (**Figure 5G**). Overall, these results suggest that OAT deficiency in the adult RPE/Cho triggers metabolic stress, impairs protein synthesis, and induces structural remodeling, potentially contributing to early RPE damage in GA (**Figure 5H**).

OAT loss in neonatal RPE/Cho alters proteins in ECM composition, trafficking, and transcriptional regulation

Proteomic analysis of RPE/Cho tissue in neonates identified 167 differentially expressed (DE)

proteins, including 82 downregulated and 85 upregulated (**Figure 6A**). Most of these DE proteins were associated with metabolism (22%), transcription (21%), signal transduction (13%), and protein homeostasis (11%) (**Figure 6B**). GO biological process analysis highlighted transcriptional regulation as the most significantly altered pathway, supported by the preferential localization of altered proteins in the nucleus and chromosomes (**Figure 6C**). Strikingly, many secreted proteins involved in ECM structure, lipid transport, and immune function were downregulated. Specifically, proline-rich ECM proteins such as COGA1, CO1A1, CO1A2, and COBA2 were substantially decreased (**Figure 6D**). Moreover, several proteins involved in intracellular transport and endosomal trafficking, including RAB6B, RFIP1, SYT5, CP131, MAST1, and TOR1A, were upregulated, whereas the melanosome trafficking protein MYRIP was downregulated (**Figure 6D**). Particularly, significant changes were observed in the nuclear proteins of the RPE/Cho in *Oat*^{rgh} mice. For instance, histone- and chromatin-modifying enzymes such as KDM5B, KDM5C, PHF2, H2B3A, H2B3B, and H2B2E, were upregulated. Consistent with this, key developmental transcription factors critical for RPE and retinal development, including HMGA1, NR2E3, VSX2, SAM11, and NR2C2, were elevated (**Figure 6E**), pointing to broad transcriptional reprogramming in these mice. Additionally, cell cycle regulators (LIFR, IFIT3) and DNA damage response proteins (BRAT1, TX264) were upregulated, further implicating nuclear involvement in the cellular response to OAT deficiency in neonatal RPE/Cho (**Table S9**).

Manual annotation of DE proteins revealed significant changes in protein homeostasis pathways, including ubiquitination (UBP30, CATC, ARI2, RBBP6, KCMF1), protein folding (TM35A, TOR1A, DNJC8), and peptidase activity (SPB12, CATC) (**Figure 6F**). Although metabolism was the top enriched pathway in neonatal RPE/Cho, we extended our exploration of metabolic proteins using GO analysis (**Table S9**). We found alterations in pathways related to visual function, ion transport, and lipid metabolism (**Figure 6G**). Phototransduction proteins such as CNGA1 and GUC2E were upregulated, along with vesicular trafficking proteins (**Figure 6D**), and lysosomal enzymes (e.g. MA2B1, AGAL). Conversely, apolipoproteins (APOA1, APOA2, APOC3) critical for systemic lipid transport were downregulated. In summary, OAT deficiency in neonatal RPE/Cho alters vesicular trafficking, protein homeostasis, and lipid metabolism, which are accompanied by significant nuclear alterations (**Figure 6K**).

Neonatal and adult RPE/Cho exhibit distinct proteomes

To investigate the age-dependent effects of OAT deficiency on RPE/Cho proteomes, we

compared neonatal and adult tissues. A total of 254 proteins were DE in the adult RPE/Cho, compared with 167 in neonates, with only six proteins (LIFR, KCMF1, CILP2, CO1A2, MYH1, MYO9B) shared between groups (**Figure 7A, B**). Both age groups featured proteomic changes associated with metabolism, signal transduction, and cytoskeletal organization. Neonates showed more pronounced alterations in transcriptional regulation and protein homeostasis, whereas adults uniquely upregulated crystallin family proteins (**Figure S7**). Remarkably, ECM-associated proteins were upregulated in adults (**Figure 5G, S7**) but downregulated in neonates (**Figure 6D, S7)**, highlighting age-dependent differences in ECM composition and tissue structure adaptations to OAT deficiency. Metabolic pathways analysis revealed that adults had nearly three times more altered metabolic proteins (98 DE proteins) than neonates (36 DE proteins). While both groups shared changes in lipid, ion transport, nucleotide, and glycan metabolism, adults presented more pronounced downregulation of detoxification, redox homeostasis, and ETC proteins (**Figure 7C**). In contrast, neonates demonstrated more substantial changes in proteins involved in lipid, ion transport, vitamin, and porphyrin metabolism (**Figure 7D**). Together, these findings demonstrate that OAT deficiency causes distinct, age-specific proteomic alterations in the RPE/Cho, shifting from transcriptional and developmental dysregulation in neonates to pronounced metabolic stress and tissue structural changes in the adult.

Cross-tissue analysis reveals distinct adult and neonatal proteomes

To investigate the age-specific effects of OAT deficiency, we compared the DE proteins across all tissues in both adult and neonate mice (**Figure 8A, B**). OAT was the only protein consistently downregulated in all three tissues at both ages, confirming the robustness of our model. The RPE/Cho showed the most extensive proteomic changes, followed by liver and retina, underscoring its role as the primary site of injury in GA[2]. Aside from OAT, six proteins were consistently altered across all three tissues at both ages. In adults, the proteins TNNT3, CP341, BGAL, and Q8HWB2 were similarly regulated in all tissues, while MYH7B and CPLX4 showed opposite regulation between the RPE/Cho and liver (**Figure 8C**). These proteins are functionally linked to cytoskeletal structure and vesicle trafficking (TNNT3, MYH7B, CPLX4), lysosomal processing (BGAL), immune signaling (Q8HWB2), and lipid metabolism (CP341), highlighting a functional link between the RPE/Cho and liver. Remarkably, fetal serum protein (FETA), a fetal protein which normally decreases after birth[41], was upregulated in all neonatal tissues (**Figure 8D**). The neonatal RPE/Cho and retina shared more proteomic changes compared to adults, including downregulation of MYRIP, a melanosome trafficking adaptor, while SP3 (a

transcriptional regulator) and CNGA1 (a rod cGMP channel subunit) were differentially regulated between these two tissues. The liver and RPE/Cho both showed upregulation of lysosomal glycosidase (MAN2B1), whereas the liver and retina had one commonly altered protein, the cholesterol biosynthesis enzyme (FDFT), which was increased in the liver but decreased in the retina. Taken together, OAT was the only protein consistently reduced across all tissues and ages, with the RPE/Cho showing the most changes, highlighting tissue- and age-specific effects of OAT deficiency on metabolism, tissue structure, and signaling pathways.

DISCUSSION

In this study, we comprehensively characterized the proteomic landscape of *Oat*^{rhg} mice in two age groups, neonates and adults, across the liver, retina, and RPE/Cho. We have demonstrated that OAT deficiency leads to diverse changes in age- and tissue-specific proteomic profiles, illustrating that OAT activity carries functional implications that extend beyond amino acid metabolism. For example, we found that OAT deficiency affects multiple key pathways, including lipid metabolism, detoxification, chromatin organization, as well as cytoskeletal and ECM remodeling. Among all tissues examined, the RPE/Cho displayed the most pronounced proteomic alterations, reinforcing its central role in the pathogenesis of GA[2]. Our findings highlight the age- and tissue-specific functions of OAT, that may account for the strikingly different impacts of its deficiency in neonates and adults.

Neonates face major metabolic challenges as they shift from continuous maternal nutrient supply to intermittent feeding while supporting rapid growth[42,43]. Unlike adults, they have limited capacity to synthesize glucose, as well as low glycogen stores, making them highly vulnerable to hypoglycemia[44,45]. As a result, neonatal metabolism relies heavily on lipid-derived fuels (milk fat, ketone bodies) and amino acids to support growth and organ development[46,47]. Our results highlight OAT as a key metabolic regulator during this critical window, as nearly 80% of altered proteins in OAT-deficient neonatal livers are linked to amino acid, lipid, and sugar metabolism. Central to this adaptation is the age-dependent shift in the direction of the OAT catalyzed reaction. During neonatal growth, the high demand for arginine[9,48], coupled with its low concentration in maternal milk[49], drives arginine synthesis from ornithine via the reverse OAT reaction[6,8,14] (**Figure 1B**). In contrast, the high-protein diet in adulthood favors the forward reaction, catabolizing ornithine to support ammonia detoxification through the urea cycle[6,8]. This metabolic shift explains our findings of low ornithine levels in neonatal tissues and elevated ornithine in adults. The resulting imbalance in substrate availability may contribute to the

hyperammonemia seen in human infants with OAT deficiency. We found significant upregulation of key urea cycle enzymes, including aspartate aminotransferase (AATC) and argininosuccinate synthase (ASSY), which likely reflects a compensatory response to prevent ammonia accumulation. Additionally, carbonic anhydrases 5a (CAH5A) and 3 (CAH3) were downregulated in the liver. A deficiency in CAH5A is known to cause hyperammonemia associated with symptoms like lethargy and poor feeding, which closely resemble the clinical features observed in human neonates with OAT deficiency[50,51].

Additionally, OAT deficiency has altered proteins of other critical metabolic pathways in the liver. We found a marked downregulation of enzymes involved in fatty acid oxidation (FABPI, OCTC, ACSS3), indicating that *Oat*^{rhg} neonates may have a reduced capacity to utilize lipid-derived energy sources. This aligns with reports of OAT upregulation in dietary-induced fatty liver diseases[52], further highlighting its role in lipid metabolism. Notably, the lipid-binding protein, alpha-fetoprotein (FETA), was markedly upregulated in all neonatal tissues. Since FETA is known to facilitate fatty acid transfer into cells, its increase likely represents a compensatory response to impaired lipid utilization[53,54]. Detoxification pathways were also broadly suppressed in both neonatal and adult livers. We found reduced levels of cytochrome P450 enzymes (CYPs), as well as conjugation enzymes, including sulfotransferases (SULTs), UDP-glucuronosyltransferases (UGTs), and glutathione S-transferases (GSTs). The reduced abundance of these enzymes impairs the clearance of xenobiotics, bilirubin, endogenous steroids, and bile acids[55–59]. Given that the detoxification capacity is inherently immature in neonates[60–62], the marked suppression of detoxification enzymes could exacerbate their susceptibility to hyperbilirubinemia and toxic metabolite accumulation, possibly contributing to neonatal lethality. Hepatic dysfunction in OAT deficiency may also compromise the liver–eye metabolic axis, which serves as a nutrient supply chain that supports retinal health[63,64]. The liver provides the eye with essential metabolites, including DHA transported via lipoproteins[65], vitamin A to support the visual cycle[66,67], taurine[68,69], and neuroprotective bile acids such as tauroursodeoxycholic acid (TUDCA)[70–72]. Our data suggest that OAT deficiency may disrupt the liver–eye axis, as reflected by significant downregulation of apolipoproteins (APOA1, APOA2, APOC3) in the neonatal RPE/Cho, potentially impairing systemic lipid transport. We speculate that liver dysfunction can make the eye more susceptible to damage, which could explain why eye is more vulnerable in GA and why gene therapies targeting the liver have been effective.

Besides metabolic disruption, our results suggest robust chromatin remodeling in *Oat*^{rhg} tissues, particularly in the neonatal RPE/Cho. Such changes may contribute to the observed alterations

in proteins involved in transcription, translation, chromatin organization, cell cycle (LIFR, IFIT3), and DNA damage response (BRAT1, TX264). These findings align with the concept of metabolic-nuclear coupling, where altered metabolites modulate the activity of chromatin-modifying enzymes and transcription factors[73–76]. This type of gene expression reprogramming is also found in various cancers, where OAT is frequently upregulated to promote cellular proliferation, invasion, and polyamine-driven tumor growth[77–80]. Further supporting this epigenetic link, we found that the neonatal *Oat*^{rhg} liver upregulated the expression of the ferritin subunits FRIL1 and FRIH, which are key regulators of iron metabolism. These changes may influence iron availability, potentially impacting iron-dependent epigenetic erasers such as Jumonji and TET demethylases[81,82]. Future metabolomics studies will be necessary to quantify changes in metabolites crucial for chromatin modification, such as acetyl-CoA, S-adenosylmethionine (SAM), α-ketoglutarate, NAD^+, and polyamines[73,74,83–85].
In both the neonatal and adult RPE/Cho, proteins linked to the ECM, cytoskeleton, and vesicular transport were significantly altered. Collagen proteins were downregulated in neonates but upregulated in adults, suggesting an age-dependent response to OAT deficiency. Given that proline- a key component of ECM components such as collagen- is synthesized from products of OAT reaction, altered proline levels observed in GA patients[32,86] highlight a metabolic link between OAT deficiency and ECM production.

The RPE consists of a highly polarized monolayer of cells, with the apical side providing an interface with the photoreceptors, and a basal surface connected to Bruch's membrane. This polarization is crucial for the directional transport of proteins, nutrients, and the daily phagocytosis of POS[37,38,87–89]. These functions rely on a well-organized cytoskeleton and its stable connections to the ECM. Any disruption of this structure compromises RPE integrity and, ultimately, photoreceptor survival, as seen in several retinal degenerative diseases, including age-related macular degeneration (AMD)[90–93]. In our study, adult RPE/Cho displayed substantial downregulation of cytoskeletal components including myosin and junctional proteins. Surprisingly, several DE myosins were identified which are not typically expressed in the ocular tissues. In contrast, keratins were upregulated, including types not normally expressed in the RPE, suggesting a phenotypic shift in the adult RPE/Cho. Together, these changes point to disrupted cell polarity and the impairment of essential RPE functions, which may ultimately compromise their ability to support the photoreceptors, potentially leading to retinal degeneration[91,94,95]. Furthermore, several GTPases governing cytoskeleton dynamics[96,97], signaling[98,99], and gene expression[98] were suppressed. We also identified

decreases in the expression of mitochondrial proteins involved in oxidative phosphorylation (e.g. CX7A1, Cox2, NDUS8), transport (TOM22, MPC1), and mitochondrial fusion (MFN1), indicating mitochondrial dysfunction and compromised energy metabolism. Moreover, mitochondria can signal to nuclei to trigger gene expression reprogramming in response to cellular stress[100–102]. Importantly, elevated ornithine has shown to be cytotoxic specifically to RPE cells[103–105], while hyperornithinemia in other contexts such as in hyperonithinemia-hyperammonemia-homocitrullinura (HHH) syndrome, does not cause retinal pathology[106–108]. This further emphasizes the importance of studying tissue-specific responses to these metabolic disturbances. Supporting the role of cellular stress, we found substantial upregulation of crystallin family members, which exert cytoprotective functions in the RPE under stress conditions[106,107]. Taken together, these widespread defects in the cytoskeleton, metabolism, and mitochondrial function underscore the vulnerability of the RPE/Cho to combined OAT deficiency and hyperornithinemia and provide mechanistic insights into progressive retinal degeneration in GA.

CONCLUSION

Our findings reveal that OAT deficiency drives distinct age- and tissue-specific proteomic alterations that extend beyond ornithine metabolism. In neonates, OAT is a central metabolic regulator, and its deficiency disrupts developmental processes and causes dysregulation in lipid metabolism and detoxification in the liver, providing a mechanistic basis for neonatal hyperammonemia and lethality. In adults, we identify the RPE/Cho as the primary site of proteomic alterations including cytoskeletal defects and reduced mitochondrial and translational capacity. This combination of structural and metabolic changes helps explain how global OAT deficiency drives tissue-specific effects at different stages, and highlight potential new pathways involved in GA pathogenesis.

LIMITATION OF THE STUDY

While our study provides an in-depth proteomic analysis and uncovers novel insights into OAT deficiency, it has some limitations. First, proteins were sampled from a single hepatic region, may not capture the full cellular and functional heterogeneity of the liver. Second, RPE and choroid were collected as a complex to better preserve RPE integrity. Future studies are required to dissect their specific changes by optimized separation techniques or spatial proteomics. Finally, our neonatal study design did not include arginine supplementation for the

Oat^{rhg} mice to avoid interference. As a result, these pups were much smaller and weaker than controls, possibly due to reduced milk intake from the mother and associated nutritional stress, which may have contributed to the observed proteomic profiles.

Author Contributions

Conceptualization: Artjola Puja, Jianhai Du
Methodology: Artjola Puja, Mark Eminhizer, Tuan Ngo, Rong Xu
Investigation (experiments/data collection): Artjola Puja, Rong Xu, Mark Eminhizer, Meghashri Saravanan
Resources (animals/samples/instrumentation): Artjola Puja, Mark Eminhizer, Tuan Ngo, Rong Xu, Qingyan Wang, Ying Zhang
Visualization (figures/tables): Artjola Puja, Meghashri Saravanan
Writing – Review & Editing: Artjola Puja, Mark Eminhizer, Tuan Ngo, Rong Xu, Qingyan Wang, Ying Zhang
Supervision: Jianhai Du
Funding Acquisition: NIH Grants (EY026030, EY031324, EY032462), the Retina Research Foundation, NIH/NIGMS grant R24GM137786 to IDeA National Resource for Quantitative Proteomics, NIH NIGMS P20GM144230 Visual Sciences COBRE grant to WVU, and an unrestricted challenge grant from Research to Prevent Blindness (RPB) to the Ophthalmology department at WVU.

Acknowledgement: This work was supported by NIH Grants (EY026030, EY031324, EY032462), the Retina Research Foundation, NIH/NIGMS grant R24GM137786 to IDeA National Resource for Quantitative Proteomics, NIH NIGMS P20GM144230 Visual Sciences COBRE grant to WVU, and an unrestricted challenge grant from Research to Prevent Blindness (RPB) to the Ophthalmology department at WVU.
We also thank Dr. David Sean Hansman, postdoctoral fellow in our laboratory, for reviewing the manuscript and providing valuable suggestions.

Data availability

The mass spectrometry proteomics data have been deposited to the ProteomeXchange Consortium via PRIDE partner repository with the dataset identifier PXD063614 and 10.6019/PXD063614.

Abbreviation: GA (gyrate atrophy), **OAT** (ornithine aminotransferase), **RPE/Cho** (retinal pigment epithelium/choroid), **TCA cycle** (tricarboxylic acid cycle), **POS** (photoreceptor outer segment), **ER** (endoplasmic reticulum), **ECM** (extracellular matrix), **GO** (Gene Ontology), **WT** (wild type), **DE** (differentially expressed).

REFERENCES:

(1) Takki, K. Gyrate Atrophy of the Choroid and Retina Associated with Hyperornithinaemia. *Br J Ophthalmol* **1974**, *58* (1), 3–23. https://doi.org/10.1136/bjo.58.1.3.

(2) Wang, T.; Milam, A. H.; Steel, G.; Valle, D. A Mouse Model of Gyrate Atrophy of the Choroid and Retina. Early Retinal Pigment Epithelium Damage and Progressive Retinal Degeneration. *J. Clin. Invest.* **1996**, *97* (12), 2753–2762. https://doi.org/10.1172/JCI118730.

(3) Valle, D.; Walser, M.; Brusilow, S.; Kaiser-Kupfer, M. I.; Takki, K. Gyrate Atrophy of the Choroid and Retina. Biochemical Considerations and Experience with an Arginine-Restricted Diet. *Ophthalmology* **1981**, *88* (4), 325–330. https://doi.org/10.1016/s0161-6420(81)35028-3.

(4) Kaiser-Kupfer, M. I.; Caruso, R. C.; Valle, D. Gyrate Atrophy of the Choroid and Retina. Long-Term Reduction of Ornithine Slows Retinal Degeneration. *Arch Ophthalmol* **1991**, *109* (11), 1539–1548. https://doi.org/10.1001/archopht.1991.01080110075039.

(5) Kaiser-Kupfer, M. I.; Ludwig, I. H.; de Monasterio, F. M.; Valle, D.; Krieger, I. Gyrate Atrophy of the Choroid and Retina. Early Findings. *Ophthalmology* **1985**, *92* (3), 394–401. https://doi.org/10.1016/s0161-6420(85)34022-8.

(6) Kaczmarczyk, A.; Baker, M.; Diddle, J.; Yuzyuk, T.; Valle, D.; Lindstrom, K. A Neonate with Ornithine Aminotransferase Deficiency; Insights on the Hyperammonemia-Associated Biochemical Phenotype of Gyrate Atrophy. *Mol Genet Metab Rep* **2022**, *31*, 100857. https://doi.org/10.1016/j.ymgmr.2022.100857.

(7) Cleary, M. A.; Dorland, L.; de Koning, T. J.; Poll-The, B. T.; Duran, M.; Mandell, R.; Shih, V. E.; Berger, R.; Olpin, S. E.; Besley, G. T. N. Ornithine Aminotransferase Deficiency: Diagnostic Difficulties in Neonatal Presentation. *J Inherit Metab Dis* **2005**, *28* (5), 673–679. https://doi.org/10.1007/s10545-005-0074-1.

(8) Wang, T.; Lawler, A. M.; Steel, G.; Sipila, I.; Milam, A. H.; Valle, D. Mice Lacking Ornithine-Delta-Aminotransferase Have Paradoxical Neonatal Hypoornithinaemia and Retinal Degeneration. *Nat Genet* **1995**, *11* (2), 185–190. https://doi.org/10.1038/ng1095-185.

(9) Riby, J. E.; Hurwitz, R. E.; Kretchmer, N. Development of Ornithine Metabolism in the Mouse Intestine. *Pediatr Res* **1990**, *28* (3), 261–265. https://doi.org/10.1203/00006450-199009000-00022.

(10) Wu, G.; Meininger, C. J.; Knabe, D. A.; Bazer, F. W.; Rhoads, J. M. Arginine Nutrition in Development, Health and Disease. *Curr Opin Clin Nutr Metab Care* **2000**, *3* (1), 59–66. https://doi.org/10.1097/00075197-200001000-00010.

(11) Kaiser-Kupfer, M. I.; Caruso, R. C.; Valle, D. Gyrate Atrophy of the Choroid and Retina: Further Experience with Long-Term Reduction of Ornithine Levels in Children. *Arch Ophthalmol* **2002**, *120* (2), 146–153. https://doi.org/10.1001/archopht.120.2.146.

(12) Jasani, K. M.; Parry, N. R. A.; Black, G.; Kelly, S. P. Unique Case of Gyrate Atrophy with a Well-Preserved Electroretinogram (ERG). *BMJ Case Rep* **2018**, *2018*, bcr2016217556. https://doi.org/10.1136/bcr-2016-217556.

(13) Doimo, M.; Desbats, M. A.; Baldoin, M. C.; Lenzini, E.; Basso, G.; Murphy, E.; Graziano, C.; Seri, M.; Burlina, A.; Sartori, G.; Trevisson, E.; Salviati, L. Functional Analysis of Missense Mutations of OAT, Causing Gyrate Atrophy of Choroid and Retina. *Hum Mutat* **2013**, *34* (1), 229–236. https://doi.org/10.1002/humu.22233.

(14) Ginguay, A.; Cynober, L.; Curis, E.; Nicolis, I. Ornithine Aminotransferase, an Important Glutamate-Metabolizing Enzyme at the Crossroads of Multiple Metabolic Pathways. *Biology (Basel)* **2017**, *6* (1), 18. https://doi.org/10.3390/biology6010018.

(15) Boffa, I.; Polishchuk, E.; De Stefano, L.; Dell'Aquila, F.; Nusco, E.; Marrocco, E.; Audano, M.; Pedretti, S.; Caterino, M.; Bellezza, I.; Ruoppolo, M.; Mitro, N.; Cellini, B.; Auricchio, A.; Brunetti-Pierri, N. Liver-Directed Gene Therapy for Ornithine Aminotransferase Deficiency. *EMBO Molecular Medicine* **2023**, *15* (4), e17033. https://doi.org/10.15252/emmm.202217033.

(16) Kuwabara, T.; Ishikawa, Y.; Kaiser-Kupfer, M. I. Experimental Model of Gyrate Atrophy in Animals. *Ophthalmology* **1981**, *88* (4), 331–335. https://doi.org/10.1016/s0161-6420(81)35027-1.

(17) Dell'Aquila, F.; Di Cunto, R.; Marrocco, E.; Del Prete, E.; D'Alessio, A.; De Stefano, L.; Notaro, S.; Nusco, E.; Auricchio, A. Combined Intraocular and Intravenous Gene Delivery for Therapy of Gyrate Atrophy of the Choroid and Retina. *Mol Ther* **2025**, *33* (7), 2997–3005. https://doi.org/10.1016/j.ymthe.2024.10.019.

(18) Bisaillon, J. J.; Radden, L. A.; Szabo, E. T.; Hughes, S. R.; Feliciano, A. M.; Nesta, A. V.; Petrovic, B.; Palanza, K. M.; Lancinskas, D.; Szmurlo, T. A.; Artus, D. C.; Kapper, M. A.; Mulrooney, J. P.; King, T. R. The Retarded Hair Growth (Rhg) Mutation in Mice Is an Allele of Ornithine Aminotransferase (Oat). *Mol Genet Metab Rep* **2014**, *1*, 378–390. https://doi.org/10.1016/j.ymgmr.2014.08.002.

(19) Zhu, S.; Yam, M.; Wang, Y.; Linton, J. D.; Grenell, A.; Hurley, J. B.; Du, J. Impact of Euthanasia, Dissection and Postmortem Delay on Metabolic Profile in Mouse Retina and RPE/Choroid. *Exp Eye Res* **2018**, *174*, 113–120. https://doi.org/10.1016/j.exer.2018.05.032.

(20) Xu, R.; Ritz, B. K.; Wang, Y.; Huang, J.; Zhao, C.; Gong, K.; Liu, X.; Du, J. The Retina and Retinal Pigment Epithelium Differ in Nitrogen Metabolism and Are Metabolically Connected. *J Biol Chem* **2020**, *295* (8), 2324–2335. https://doi.org/10.1074/jbc.RA119.011727.

(21) Searle, B. C.; Pino, L. K.; Egertson, J. D.; Ting, Y. S.; Lawrence, R. T.; MacLean, B. X.; Villén, J.; MacCoss, M. J. Chromatogram Libraries Improve Peptide Detection and Quantification by Data Independent Acquisition Mass Spectrometry. *Nat Commun* **2018**, *9* (1), 5128. https://doi.org/10.1038/s41467-018-07454-w.

(22) Graw, S.; Tang, J.; Zafar, M. K.; Byrd, A. K.; Bolden, C.; Peterson, E. C.; Byrum, S. D. proteiNorm - A User-Friendly Tool for Normalization and Analysis of TMT and Label-Free Protein Quantification. *ACS Omega* **2020**, *5* (40), 25625–25633. https://doi.org/10.1021/acsomega.0c02564.

(23) Bolstad, B. M.; Irizarry, R. A.; Astrand, M.; Speed, T. P. A Comparison of Normalization Methods for High Density Oligonucleotide Array Data Based on Variance and Bias. *Bioinformatics* **2003**, *19* (2), 185–193. https://doi.org/10.1093/bioinformatics/19.2.185.

(24) Ritchie, M. E.; Phipson, B.; Wu, D.; Hu, Y.; Law, C. W.; Shi, W.; Smyth, G. K. Limma Powers Differential Expression Analyses for RNA-Sequencing and Microarray Studies. *Nucleic Acids Res* **2015**, *43* (7), e47. https://doi.org/10.1093/nar/gkv007.

(25) Thurman, T. J.; Washam, C. L.; Alkam, D.; Bird, J. T.; Gies, A.; Dhusia, K.; Ii, M. S. R.; Byrum, S. D. proteoDA: A Package for Quantitative Proteomics. *JOSS* **2023**, *8* (85), 5184. https://doi.org/10.21105/joss.05184.

(26) Szklarczyk, D.; Kirsch, R.; Koutrouli, M.; Nastou, K.; Mehryary, F.; Hachilif, R.; Gable, A. L.; Fang, T.; Doncheva, N. T.; Pyysalo, S.; Bork, P.; Jensen, L. J.; von Mering, C. The STRING Database in 2023: Protein-Protein Association Networks and Functional Enrichment Analyses for Any Sequenced Genome of Interest. *Nucleic Acids Res* **2023**, *51* (D1), D638–D646. https://doi.org/10.1093/nar/gkac1000.

(27) Sherman, B. T.; Hao, M.; Qiu, J.; Jiao, X.; Baseler, M. W.; Lane, H. C.; Imamichi, T.; Chang, W. DAVID: A Web Server for Functional Enrichment Analysis and Functional Annotation of Gene Lists (2021 Update). *Nucleic Acids Res* **2022**, *50* (W1), W216–W221. https://doi.org/10.1093/nar/gkac194.

(28) Heberle, H.; Meirelles, G. V.; Da Silva, F. R.; Telles, G. P.; Minghim, R. InteractiVenn: A Web-Based Tool for the Analysis of Sets through Venn Diagrams. *BMC Bioinformatics* **2015**, *16* (1), 169. https://doi.org/10.1186/s12859-015-0611-3.

(29) Li, B.; Zhang, T.; Liu, W.; Wang, Y.; Xu, R.; Zeng, S.; Zhang, R.; Zhu, S.; Gillies, M. C.; Zhu, L.; Du, J. Metabolic Features of Mouse and Human Retinas: Rods versus Cones, Macula versus Periphery, Retina versus RPE. *iScience* **2020**, *23* (11), 101672. https://doi.org/10.1016/j.isci.2020.101672.

(30) Saravanan, M.; Xu, R.; Roby, O.; Wang, Y.; Zhu, S.; Lu, A.; Du, J. Tissue-Specific Sex Difference in Mouse Eye and Brain Metabolome Under Fed and Fasted States. *Invest Ophthalmol Vis Sci* **2023**, *64* (3), 18. https://doi.org/10.1167/iovs.64.3.18.

(31) Zhu, S.; Huang, J.; Xu, R.; Wang, Y.; Wan, Y.; McNeel, R.; Parker, E.; Kolson, D.; Yam, M.; Webb, B.; Zhao, C.; Sigado, J.; Du, J. Isocitrate Dehydrogenase 3b Is Required for Spermiogenesis but Dispensable for Retinal Viability. *J Biol Chem* **2022**, *298* (9), 102387. https://doi.org/10.1016/j.jbc.2022.102387.

(32) de Sain-van der Velden, M. G. M.; Rinaldo, P.; Elvers, B.; Henderson, M.; Walter, J. H.; Prinsen, B. H. C. M. T.; Verhoeven-Duif, N. M.; de Koning, T. J.; van Hasselt, P. The Proline/Citrulline Ratio as a Biomarker for OAT Deficiency in Early Infancy. *JIMD Rep* **2012**, *6*, 95–99. https://doi.org/10.1007/8904_2011_122.

(33) Choi, J.; Li, J.; Ferdous, S.; Liang, Q.; Moffitt, J. R.; Chen, R. Spatial Organization of the Mouse Retina at Single Cell Resolution by MERFISH. *Nat Commun* **2023**, *14* (1), 4929. https://doi.org/10.1038/s41467-023-40674-3.

(34) Zhang, J.; Roberts, J. M.; Chang, F.; Schwakopf, J.; Vetter, M. L. Jarid2 Promotes Temporal Progression of Retinal Progenitors via Repression of Foxp1. *Cell Rep* **2023**, *42* (3), 112237. https://doi.org/10.1016/j.celrep.2023.112237.

(35) Fujimura, N. WNT/β-Catenin Signaling in Vertebrate Eye Development. *Front Cell Dev Biol* **2016**, *4*, 138. https://doi.org/10.3389/fcell.2016.00138.

(36) Labbé, P.; Faure, E.; Lecointe, S.; Le Scouarnec, S.; Kyndt, F.; Marrec, M.; Le Tourneau, T.; Offmann, B.; Duplaà, C.; Zaffran, S.; Schott, J. J.; Merot, J. The Alternatively Spliced LRRFIP1 Isoform-1 Is a Key Regulator of the Wnt/β-Catenin Transcription Pathway. *Biochim Biophys Acta Mol Cell Res* **2017**, *1864* (7), 1142–1152. https://doi.org/10.1016/j.bbamcr.2017.03.008.

(37) Zhu, S.; Xu, R.; Engel, A. L.; Wang, Y.; McNeel, R.; Hurley, J. B.; Chao, J. R.; Du, J. Proline Provides a Nitrogen Source in the Retinal Pigment Epithelium to Synthesize and Export Amino Acids for the Neural Retina. *bioRxiv* **2023**, 2023.04.18.537355. https://doi.org/10.1101/2023.04.18.537355.

(38) Hurley, J. B. Retina Metabolism and Metabolism in the Pigmented Epithelium: A Busy Intersection. *Annu Rev Vis Sci* **2021**, *7*, 665–692. https://doi.org/10.1146/annurev-vision-100419-115156.
(39) Markitantova, Y.; Simirskii, V. Retinal Pigment Epithelium Under Oxidative Stress: Chaperoning Autophagy and Beyond. *Int J Mol Sci* **2025**, *26* (3), 1193. https://doi.org/10.3390/ijms26031193.
(40) Kannan, R.; Sreekumar, P. G.; Hinton, D. R. Alpha Crystallins in the Retinal Pigment Epithelium and Implications for the Pathogenesis and Treatment of Age-Related Macular Degeneration. *Biochim Biophys Acta* **2016**, *1860* (1 Pt B), 258–268. https://doi.org/10.1016/j.bbagen.2015.05.016.
(41) Spear, B. T. Alpha-Fetoprotein Gene Regulation: Lessons from Transgenic Mice. *Semin Cancer Biol* **1999**, *9* (2), 109–116. https://doi.org/10.1006/scbi.1998.0087.
(42) White, R. B.; Biérinx, A.-S.; Gnocchi, V. F.; Zammit, P. S. Dynamics of Muscle Fibre Growth during Postnatal Mouse Development. *BMC Dev Biol* **2010**, *10*, 21. https://doi.org/10.1186/1471-213X-10-21.
(43) Jung, E.; Czajka-Narins, D. M. Birth Weight Doubling and Tripling Times: An Updated Look at the Effects of Birth Weight, Sex, Race and Type of Feeding. *Am J Clin Nutr* **1985**, *42* (2), 182–189. https://doi.org/10.1093/ajcn/42.2.182.
(44) Tas, E.; Garibaldi, L.; Muzumdar, R. Glucose Homeostasis in Newborns: An Endocrinology Perspective. *Neoreviews* **2020**, *21* (1), e14–e29. https://doi.org/10.1542/neo.21-1-e14.
(45) Amendoeira, S.; McNair, C.; Saini, J.; Habib, S. Glucose Homeostasis and the Neonatal Brain: A Sweet Relationship. *Neonatal Netw* **2020**, *39* (3), 137–146. https://doi.org/10.1891/0730-0832.39.3.137.
(46) Delplanque, B.; Gibson, R.; Koletzko, B.; Lapillonne, A.; Strandvik, B. Lipid Quality in Infant Nutrition: Current Knowledge and Future Opportunities. *J Pediatr Gastroenterol Nutr* **2015**, *61* (1), 8–17. https://doi.org/10.1097/MPG.0000000000000818.
(47) Mazzocchi, A.; D'Oria, V.; De Cosmi, V.; Bettocchi, S.; Milani, G. P.; Silano, M.; Agostoni, C. The Role of Lipids in Human Milk and Infant Formulae. *Nutrients* **2018**, *10* (5), 567. https://doi.org/10.3390/nu10050567.
(48) Tomlinson, C.; Rafii, M.; Sgro, M.; Ball, R. O.; Pencharz, P. Arginine Is Synthesized from Proline, Not Glutamate, in Enterally Fed Human Preterm Neonates. *Pediatr Res* **2011**, *69* (1), 46–50. https://doi.org/10.1203/PDR.0b013e3181fc6ab7.
(49) Wu, G.; Knabe, D. A.; Kim, S. W. Arginine Nutrition in Neonatal Pigs. *J Nutr* **2004**, *134* (10 Suppl), 2783S-2790S; discussion 2796S-2797S. https://doi.org/10.1093/jn/134.10.2783S.
(50) van Karnebeek, C. D.; Sly, W. S.; Ross, C. J.; Salvarinova, R.; Yaplito-Lee, J.; Santra, S.; Shyr, C.; Horvath, G. A.; Eydoux, P.; Lehman, A. M.; Bernard, V.; Newlove, T.; Ukpeh, H.; Chakrapani, A.; Preece, M. A.; Ball, S.; Pitt, J.; Vallance, H. D.; Coulter-Mackie, M.; Nguyen, H.; Zhang, L.-H.; Bhavsar, A. P.; Sinclair, G.; Waheed, A.; Wasserman, W. W.; Stockler-Ipsiroglu, S. Mitochondrial Carbonic Anhydrase VA Deficiency Resulting from CA5A Alterations Presents with Hyperammonemia in Early Childhood. *Am J Hum Genet* **2014**, *94* (3), 453–461. https://doi.org/10.1016/j.ajhg.2014.01.006.
(51) Mani Urmila, N.; Kewalramani, D.; Balakrishnan, U.; Manokaran, R. K. A Case of Carbonic Anhydrase Type VA Deficiency Presenting as West Syndrome in an Infant with

a Novel Mutation in the CA-VA Gene. *Epilepsy Behav Rep* **2022**, *20*, 100573. https://doi.org/10.1016/j.ebr.2022.100573.
(52) Luo, M.; Mengos, A. E.; Stubblefield, T. M.; Mandarino, L. J. High Fat Diet-Induced Changes in Hepatic Protein Abundance in Mice. *J Proteomics Bioinform* **2012**, *5* (3), 60–66. https://doi.org/10.4172/jpb.1000214.
(53) Calvo, M.; Naval, J.; Lampreave, F.; Uriel, J.; Piñeiro, A. Fatty Acids Bound to Alpha-Fetoprotein and Albumin during Rat Development. *Biochim Biophys Acta* **1988**, *959* (3), 238–246. https://doi.org/10.1016/0005-2760(88)90196-8.
(54) Aussel, C.; Masseyeff, R. Human Alpha-Fetoprotein-Fatty Acid Interaction. *Biochem Biophys Res Commun* **1983**, *115* (1), 38–45. https://doi.org/10.1016/0006-291x(83)90965-8.
(55) Esteves, F.; Rueff, J.; Kranendonk, M. The Central Role of Cytochrome P450 in Xenobiotic Metabolism-A Brief Review on a Fascinating Enzyme Family. *J Xenobiot* **2021**, *11* (3), 94–114. https://doi.org/10.3390/jox11030007.
(56) Fujiwara, R.; Maruo, Y.; Chen, S.; Tukey, R. H. Role of Extrahepatic UDP-Glucuronosyltransferase 1A1: Advances in Understanding Breast Milk-Induced Neonatal Hyperbilirubinemia. *Toxicol Appl Pharmacol* **2015**, *289* (1), 124–132. https://doi.org/10.1016/j.taap.2015.08.018.
(57) Tukey, R. H.; Strassburg, C. P. Human UDP-Glucuronosyltransferases: Metabolism, Expression, and Disease. *Annu Rev Pharmacol Toxicol* **2000**, *40*, 581–616. https://doi.org/10.1146/annurev.pharmtox.40.1.581.
(58) Alnouti, Y. Bile Acid Sulfation: A Pathway of Bile Acid Elimination and Detoxification. *Toxicol Sci* **2009**, *108* (2), 225–246. https://doi.org/10.1093/toxsci/kfn268.
(59) Sharma, R.; Yang, Y.; Sharma, A.; Awasthi, S.; Awasthi, Y. C. Antioxidant Role of Glutathione S-Transferases: Protection against Oxidant Toxicity and Regulation of Stress-Mediated Apoptosis. *Antioxid Redox Signal* **2004**, *6* (2), 289–300. https://doi.org/10.1089/152308604322899350.
(60) Coughtrie, M. W. H. Ontogeny of Human Conjugating Enzymes. *Drug Metab Lett* **2015**, *9* (2), 99–108. https://doi.org/10.2174/1872312809666150602151213.
(61) Hines, R. N. Ontogeny of Human Hepatic Cytochromes P450. *J Biochem Mol Toxicol* **2007**, *21* (4), 169–175. https://doi.org/10.1002/jbt.20179.
(62) Mathew, J.; Cattan, A. R.; Hall, A. G.; Hines, J. E.; Nelson, R.; Eastham, E.; Burt, A. D. Glutathione S-Transferases in Neonatal Liver Disease. *J Clin Pathol* **1992**, *45* (8), 679–683. https://doi.org/10.1136/jcp.45.8.679.
(63) Wu, J.; Duan, C.; Yang, Y.; Wang, Z.; Tan, C.; Han, C.; Hou, X. Insights into the Liver-Eyes Connections, from Epidemiological, Mechanical Studies to Clinical Translation. *J Transl Med* **2023**, *21* (1), 712. https://doi.org/10.1186/s12967-023-04543-3.
(64) Yuan, T.-H.; Yue, Z.-S.; Zhang, G.-H.; Wang, L.; Dou, G.-R. Beyond the Liver: Liver-Eye Communication in Clinical and Experimental Aspects. *Front Mol Biosci* **2021**, *8*, 823277. https://doi.org/10.3389/fmolb.2021.823277.
(65) Scott, B. L.; Bazan, N. G. Membrane Docosahexaenoate Is Supplied to the Developing Brain and Retina by the Liver. *Proc Natl Acad Sci U S A* **1989**, *86* (8), 2903–2907. https://doi.org/10.1073/pnas.86.8.2903.
(66) Berry, D. C.; Jacobs, H.; Marwarha, G.; Gely-Pernot, A.; O'Byrne, S. M.; DeSantis, D.; Klopfenstein, M.; Feret, B.; Dennefeld, C.; Blaner, W. S.; Croniger, C. M.; Mark, M.; Noy, N.; Ghyselinck, N. B. The STRA6 Receptor Is Essential for Retinol-Binding Protein-

Induced Insulin Resistance but Not for Maintaining Vitamin A Homeostasis in Tissues Other than the Eye. *J Biol Chem* **2013**, *288* (34), 24528–24539. https://doi.org/10.1074/jbc.M113.484014.

(67) Steinhoff, J. S.; Lass, A.; Schupp, M. Retinoid Homeostasis and Beyond: How Retinol Binding Protein 4 Contributes to Health and Disease. *Nutrients* **2022**, *14* (6), 1236. https://doi.org/10.3390/nu14061236.

(68) Singh, C.; Hoppe, G.; Tran, V.; McCollum, L.; Bolok, Y.; Song, W.; Sharma, A.; Brunengraber, H.; Sears, J. E. Serine and 1-Carbon Metabolism Are Required for HIF-Mediated Protection against Retinopathy of Prematurity. *JCI Insight* **2019**, *4* (14), e129398, 129398. https://doi.org/10.1172/jci.insight.129398.

(69) García-Ayuso, D.; Di Pierdomenico, J.; Martínez-Vacas, A.; Vidal-Sanz, M.; Picaud, S.; Villegas-Pérez, M. P. Taurine: A Promising Nutraceutic in the Prevention of Retinal Degeneration. *Neural Regen Res* **2024**, *19* (3), 606–610. https://doi.org/10.4103/1673-5374.380820.

(70) Mantopoulos, D.; Murakami, Y.; Comander, J.; Thanos, A.; Roh, M.; Miller, J. W.; Vavvas, D. G. Tauroursodeoxycholic Acid (TUDCA) Protects Photoreceptors from Cell Death after Experimental Retinal Detachment. *PLoS One* **2011**, *6* (9), e24245. https://doi.org/10.1371/journal.pone.0024245.

(71) Fernández-Sánchez, L.; Lax, P.; Pinilla, I.; Martín-Nieto, J.; Cuenca, N. Tauroursodeoxycholic Acid Prevents Retinal Degeneration in Transgenic P23H Rats. *Invest Ophthalmol Vis Sci* **2011**, *52* (8), 4998–5008. https://doi.org/10.1167/iovs.11-7496.

(72) Lawson, E. C.; Bhatia, S. K.; Han, M. K.; Aung, M. H.; Ciavatta, V.; Boatright, J. H.; Pardue, M. T. Tauroursodeoxycholic Acid Protects Retinal Function and Structure in Rd1 Mice. *Adv Exp Med Biol* **2016**, *854*, 431–436. https://doi.org/10.1007/978-3-319-17121-0_57.

(73) Sabari, B. R.; Zhang, D.; Allis, C. D.; Zhao, Y. Metabolic Regulation of Gene Expression through Histone Acylations. *Nat Rev Mol Cell Biol* **2017**, *18* (2), 90–101. https://doi.org/10.1038/nrm.2016.140.

(74) Schvartzman, J. M.; Thompson, C. B.; Finley, L. W. S. Metabolic Regulation of Chromatin Modifications and Gene Expression. *J Cell Biol* **2018**, *217* (7), 2247–2259. https://doi.org/10.1083/jcb.201803061.

(75) Boon, R. Metabolic Fuel for Epigenetic: Nuclear Production Meets Local Consumption. *Front Genet* **2021**, *12*, 768996. https://doi.org/10.3389/fgene.2021.768996.

(76) Todisco, S.; Iacobazzi, D.; Santarsiero, A.; Convertini, P.; Infantino, V. Nuclear Functional Role of Metabolic Enzymes and Related Metabolites: Focus on Gene Expression Regulation. *Mol Metab* **2025**, *100*, 102233. https://doi.org/10.1016/j.molmet.2025.102233.

(77) Lee, M.-S.; Dennis, C.; Naqvi, I.; Dailey, L.; Lorzadeh, A.; Ye, G.; Zaytouni, T.; Adler, A.; Hitchcock, D. S.; Lin, L.; Hoffman, M. T.; Bhuiyan, A. M.; Barth, J. L.; Machacek, M. E.; Mino-Kenudson, M.; Dougan, S. K.; Jadhav, U.; Clish, C. B.; Kalaany, N. Y. Ornithine Aminotransferase Supports Polyamine Synthesis in Pancreatic Cancer. *Nature* **2023**, *616* (7956), 339–347. https://doi.org/10.1038/s41586-023-05891-2.

(78) Jiang, Z.; Wei, C.; Luo, Y.; Xiao, Y.; Wang, L.; Guo, W.; Yuan, X. Ornithine Aminotransferase and Carbamoyl Phosphate Synthetase 1 Involved in Ammonia Metabolism Serve as Novel Targets for Early Stages of Gastric Cancer. *J Clin Lab Anal* **2022**, *36* (10), e24692. https://doi.org/10.1002/jcla.24692.

(79) Liu, Y.; Wu, L.; Li, K.; Liu, F.; Wang, L.; Zhang, D.; Zhou, J.; Ma, X.; Wang, S.; Yang, S. Ornithine Aminotransferase Promoted the Proliferation and Metastasis of Non-Small Cell Lung Cancer via Upregulation of miR-21. *J Cell Physiol* **2019**, *234* (8), 12828–12838. https://doi.org/10.1002/jcp.27939.
(80) Zigmond, E.; Ben Ya'acov, A.; Lee, H.; Lichtenstein, Y.; Shalev, Z.; Smith, Y.; Zolotarov, L.; Ziv, E.; Kalman, R.; Le, H. V.; Lu, H.; Silverman, R. B.; Ilan, Y. Suppression of Hepatocellular Carcinoma by Inhibition of Overexpressed Ornithine Aminotransferase. *ACS Med Chem Lett* **2015**, *6* (8), 840–844. https://doi.org/10.1021/acsmedchemlett.5b00153.
(81) Inoue, H.; Hanawa, N.; Katsumata, S.-I.; Aizawa, Y.; Katsumata-Tsuboi, R.; Tanaka, M.; Takahashi, N.; Uehara, M. Iron Deficiency Negatively Regulates Protein Methylation via the Downregulation of Protein Arginine Methyltransferase. *Heliyon* **2020**, *6* (10), e05059. https://doi.org/10.1016/j.heliyon.2020.e05059.
(82) Farida, B.; Ibrahim, K. G.; Abubakar, B.; Malami, I.; Bello, M. B.; Abubakar, M. B.; Abbas, A. Y.; Imam, M. U. Iron Deficiency and Its Epigenetic Effects on Iron Homeostasis. *J Trace Elem Med Biol* **2023**, *78*, 127203. https://doi.org/10.1016/j.jtemb.2023.127203.
(83) Pirini, F.; Ferrari, A.; Jandoubi, M.; Azzali, I.; Angeli, D.; Mondrone, R.; Bracci, C.; Ruggieri, F.; Martinelli, G.; Simonetti, G. Polyamines at the Crossroad between Cell Metabolism and Epigenetic Regulation in Acute Leukemias. *Cell Death Discov* **2025**, *11* (1), 301. https://doi.org/10.1038/s41420-025-02573-y.
(84) Song, H.; Shen, R.; Liu, X.; Yang, X.; Xie, K.; Guo, Z.; Wang, D. Histone Post-Translational Modification and the DNA Damage Response. *Genes Dis* **2023**, *10* (4), 1429–1444. https://doi.org/10.1016/j.gendis.2022.04.002.
(85) Sakamoto, A.; Terui, Y.; Uemura, T.; Igarashi, K.; Kashiwagi, K. Polyamines Regulate Gene Expression by Stimulating Translation of Histone Acetyltransferase mRNAs. *J Biol Chem* **2020**, *295* (26), 8736–8745. https://doi.org/10.1074/jbc.RA120.013833.
(86) Balfoort, B. M.; Buijs, M. J. N.; ten Asbroek, A. L. M. A.; Bergen, A. A. B.; Boon, C. J. F.; Ferreira, E. A.; Houtkooper, R. H.; Wagenmakers, M. A. E. M.; Wanders, R. J. A.; Waterham, H. R.; Timmer, C.; van Karnebeek, C. D.; Brands, M. M. A Review of Treatment Modalities in Gyrate Atrophy of the Choroid and Retina (GACR). *Molecular Genetics and Metabolism* **2021**, *134* (1), 96–116. https://doi.org/10.1016/j.ymgme.2021.07.010.
(87) Caceres, P. S.; Rodriguez-Boulan, E. Retinal Pigment Epithelium Polarity in Health and Blinding Diseases. *Curr Opin Cell Biol* **2020**, *62*, 37–45. https://doi.org/10.1016/j.ceb.2019.08.001.
(88) Kay, P.; Yang, Y. C.; Paraoan, L. Directional Protein Secretion by the Retinal Pigment Epithelium: Roles in Retinal Health and the Development of Age-Related Macular Degeneration. *J Cell Mol Med* **2013**, *17* (7), 833–843. https://doi.org/10.1111/jcmm.12070.
(89) Hansman, D. S.; Du, J.; Casson, R. J.; Peet, D. J. Eye on the Horizon: The Metabolic Landscape of the RPE in Aging and Disease. *Prog Retin Eye Res* **2025**, *104*, 101306. https://doi.org/10.1016/j.preteyeres.2024.101306.
(90) Bhutto, I.; Lutty, G. Understanding Age-Related Macular Degeneration (AMD): Relationships between the Photoreceptor/Retinal Pigment Epithelium/Bruch's

Membrane/Choriocapillaris Complex. *Mol Aspects Med* **2012**, *33* (4), 295–317. https://doi.org/10.1016/j.mam.2012.04.005.
(91) Piskova, T.; Kozyrina, A. N.; Di Russo, J. Mechanobiological Implications of Age-Related Remodelling in the Outer Retina. *Biomater Adv* **2023**, *147*, 213343. https://doi.org/10.1016/j.bioadv.2023.213343.
(92) Beatty, S.; Koh, H.; Phil, M.; Henson, D.; Boulton, M. The Role of Oxidative Stress in the Pathogenesis of Age-Related Macular Degeneration. *Surv Ophthalmol* **2000**, *45* (2), 115–134. https://doi.org/10.1016/s0039-6257(00)00140-5.
(93) Ach, T.; Tolstik, E.; Messinger, J. D.; Zarubina, A. V.; Heintzmann, R.; Curcio, C. A. Lipofuscin Redistribution and Loss Accompanied by Cytoskeletal Stress in Retinal Pigment Epithelium of Eyes with Age-Related Macular Degeneration. *Invest Ophthalmol Vis Sci* **2015**, *56* (5), 3242–3252. https://doi.org/10.1167/iovs.14-16274.
(94) Grisanti, S.; Guidry, C. Transdifferentiation of Retinal Pigment Epithelial Cells from Epithelial to Mesenchymal Phenotype. *Invest Ophthalmol Vis Sci* **1995**, *36* (2), 391–405.
(95) Tarau, I.-S.; Berlin, A.; Curcio, C. A.; Ach, T. The Cytoskeleton of the Retinal Pigment Epithelium: From Normal Aging to Age-Related Macular Degeneration. *Int J Mol Sci* **2019**, *20* (14), 3578. https://doi.org/10.3390/ijms20143578.
(96) Zihni, C. Phagocytosis by the Retinal Pigment Epithelium: New Insights into Polarized Cell Mechanics. *BioEssays* **2025**, *47* (1), 2300197. https://doi.org/10.1002/bies.202300197.
(97) Wittchen, E. S.; Hartnett, M. E. The Small GTPase Rap1 Is a Novel Regulator of RPE Cell Barrier Function. *Invest Ophthalmol Vis Sci* **2011**, *52* (10), 7455–7463. https://doi.org/10.1167/iovs.11-7295.
(98) Wang, H.; Jiang, Y.; Shi, D.; Quilliam, L. A.; Chrzanowska-Wodnicka, M.; Wittchen, E. S.; Li, D. Y.; Hartnett, M. E. Activation of Rap1 Inhibits NADPH Oxidase-Dependent ROS Generation in Retinal Pigment Epithelium and Reduces Choroidal Neovascularization. *FASEB J* **2014**, *28* (1), 265–274. https://doi.org/10.1096/fj.13-240028.
(99) Glotin, A.-L.; Calipel, A.; Brossas, J.-Y.; Faussat, A.-M.; Tréton, J.; Mascarelli, F. Sustained versus Transient ERK1/2 Signaling Underlies the Anti- and Proapoptotic Effects of Oxidative Stress in Human RPE Cells. *Invest Ophthalmol Vis Sci* **2006**, *47* (10), 4614–4623. https://doi.org/10.1167/iovs.06-0297.
(100) Kaarniranta, K.; Uusitalo, H.; Blasiak, J.; Felszeghy, S.; Kannan, R.; Kauppinen, A.; Salminen, A.; Sinha, D.; Ferrington, D. Mechanisms of Mitochondrial Dysfunction and Their Impact on Age-Related Macular Degeneration. *Prog Retin Eye Res* **2020**, *79*, 100858. https://doi.org/10.1016/j.preteyeres.2020.100858.
(101) Andréasson, C.; Ott, M.; Büttner, S. Mitochondria Orchestrate Proteostatic and Metabolic Stress Responses. *EMBO Rep* **2019**, *20* (10), e47865. https://doi.org/10.15252/embr.201947865.
(102) Kaarniranta, K.; Uusitalo, H.; Blasiak, J.; Felszeghy, S.; Kannan, R.; Kauppinen, A.; Salminen, A.; Sinha, D.; Ferrington, D. Mechanisms of Mitochondrial Dysfunction and Their Impact on Age-Related Macular Degeneration. *Prog Retin Eye Res* **2020**, *79*, 100858. https://doi.org/10.1016/j.preteyeres.2020.100858.
(103) Ueda, M.; Masu, Y.; Ando, A.; Maeda, H.; Del Monte, M. A.; Uyama, M.; Ito, S. Prevention of Ornithine Cytotoxicity by Proline in Human Retinal Pigment Epithelial Cells. *Invest Ophthalmol Vis Sci* **1998**, *39* (5), 820–827.

(104) Ishikawa, Y.; Kuwabara, T.; Kaiser-Kupfer, M. I. Toxic Effects of Ornithine and Its Related Compounds on the Retina. *Adv Exp Med Biol* **1982**, *153*, 371–378. https://doi.org/10.1007/978-1-4757-6903-6_46.
(105) Ando, A.; Ueda, M.; Uyama, M.; Masu, Y.; Okumura, T.; Ito, S. Heterogeneity in Ornithine Cytotoxicity of Bovine Retinal Pigment Epithelial Cells in Primary Culture. *Exp Eye Res* **2000**, *70* (1), 89–96. https://doi.org/10.1006/exer.1999.0750.
(106) Koike, R.; Fujimori, K.; Yuasa, T.; Miyatake, T.; Inoue, I.; Saheki, T. Hyperornithinemia, Hyperammonemia, and Homocitrullinuria: Case Report and Biochemical Study. *Neurology* **1987**, *37* (11), 1813–1815. https://doi.org/10.1212/wnl.37.11.1813.
(107) Shih, V. E.; Efron, M. L.; Moser, H. W. Hyperornithinemia, Hyperammonemia, and Homocitrullinuria. A New Disorder of Amino Acid Metabolism Associated with Myoclonic Seizures and Mental Retardation. *Am J Dis Child* **1969**, *117* (1), 83–92.
(108) Hommes, F. A.; Roesel, R. A.; Metoki, K.; Hartlage, P. L.; Dyken, P. R. Studies on a Case of HHH-Syndrome (Hyperammonemia, Hyperornithinemia, Homocitrullinuria). *Neuropediatrics* **1986**, *17* (1), 48–52. https://doi.org/10.1055/s-2008-1052499.
(109) Böhm, M. R. R.; Melkonyan, H.; Oellers, P.; Thanos, S. Effects of Crystallin-β-B2 on Stressed RPE in Vitro and in Vivo. *Graefes Arch Clin Exp Ophthalmol* **2013**, *251* (1), 63–79. https://doi.org/10.1007/s00417-012-2157-7.
(110) Kannan, R.; Sreekumar, P. G.; Hinton, D. R. Novel Roles for α-Crystallins in Retinal Function and Disease. *Prog Retin Eye Res* **2012**, *31* (6), 576–604. https://doi.org/10.1016/j.preteyeres.2012.06.001.

Figures and Figure legends

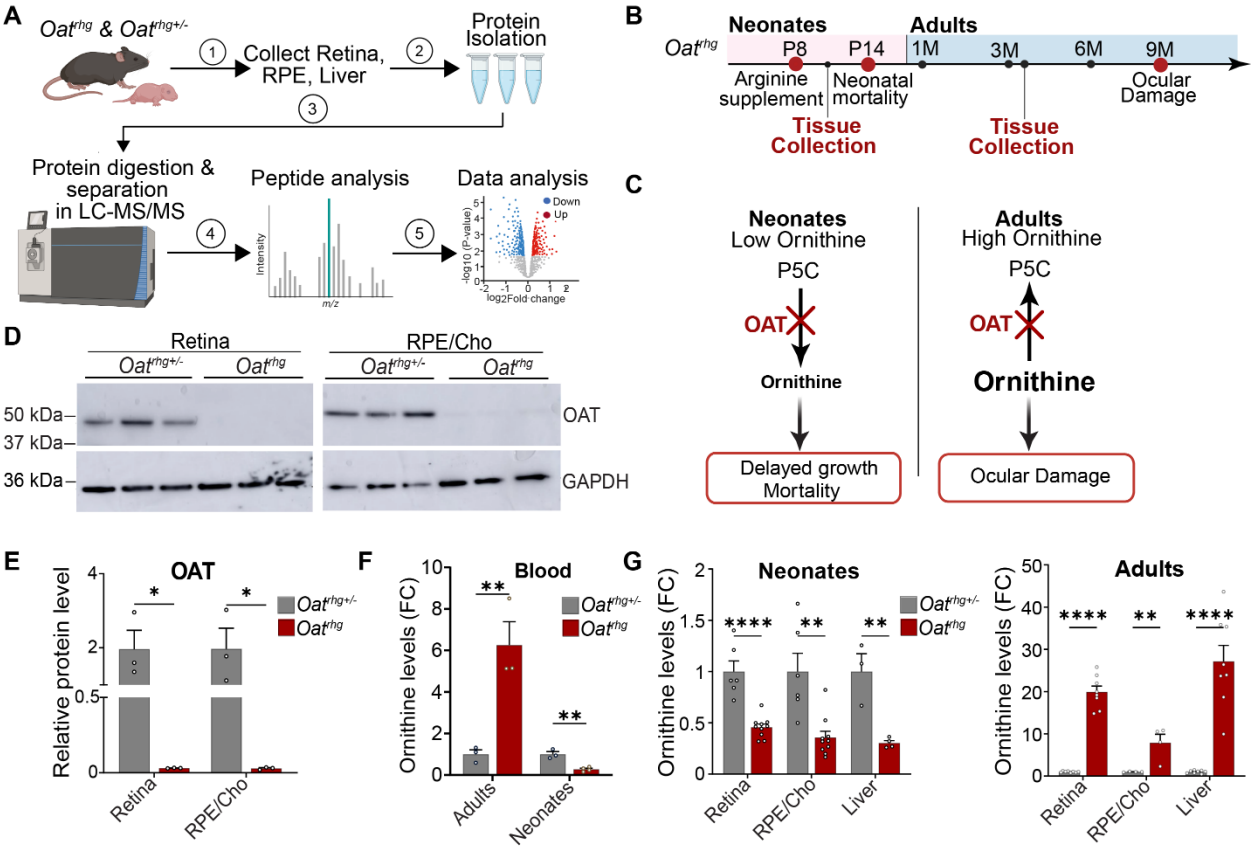

Figure 1. OAT loss causes opposite tissue and plasma ornithine levels in neonates and adults (A) Schematic overview of the workflow for proteomics analysis. **(B)** Timeline of *Oat*^{rhg} mutant mice showing key phenotypic events marked in red dots from neonatal to adult stages, and tissue collection time points. **(C)** Schematic illustration of the different role of OAT deficiency in neonates versus adults: low ornithine in neonates but acculated ornithine in adults. **(D)** Immunoblot confirming deficiency of OAT protein expression in *Oat*^{rhg} retina and RPE/Cho tissues compared to *Oat*$^{rhg+/-}$ and corresponding quantification **(E)** normalized to GAPDH loading control (N=3). **(F-G)** ornithine levels in blood, retina, RPE/Cho, and liver of *Oat*^{rhg} compared to *Oat*$^{rhg+/-}$ adult and neonate mice (N>3). All values are presented as mean ± SD. *$p < 0.05$, **$p < 0.01$, ***$p < 0.001$, ****$p < 0.0001$. Liquid Chromatography–Tandem Mass Spectrometry (LC-MS/MS); Postnatal days (P); RPE/Choroid (RPE/Cho); Pyrroline-5-carboxylate (P5C); Ornithine aminotransferase (OAT); Glyceraldehyde 3-phosphate dehydrogenase (GAPDH).

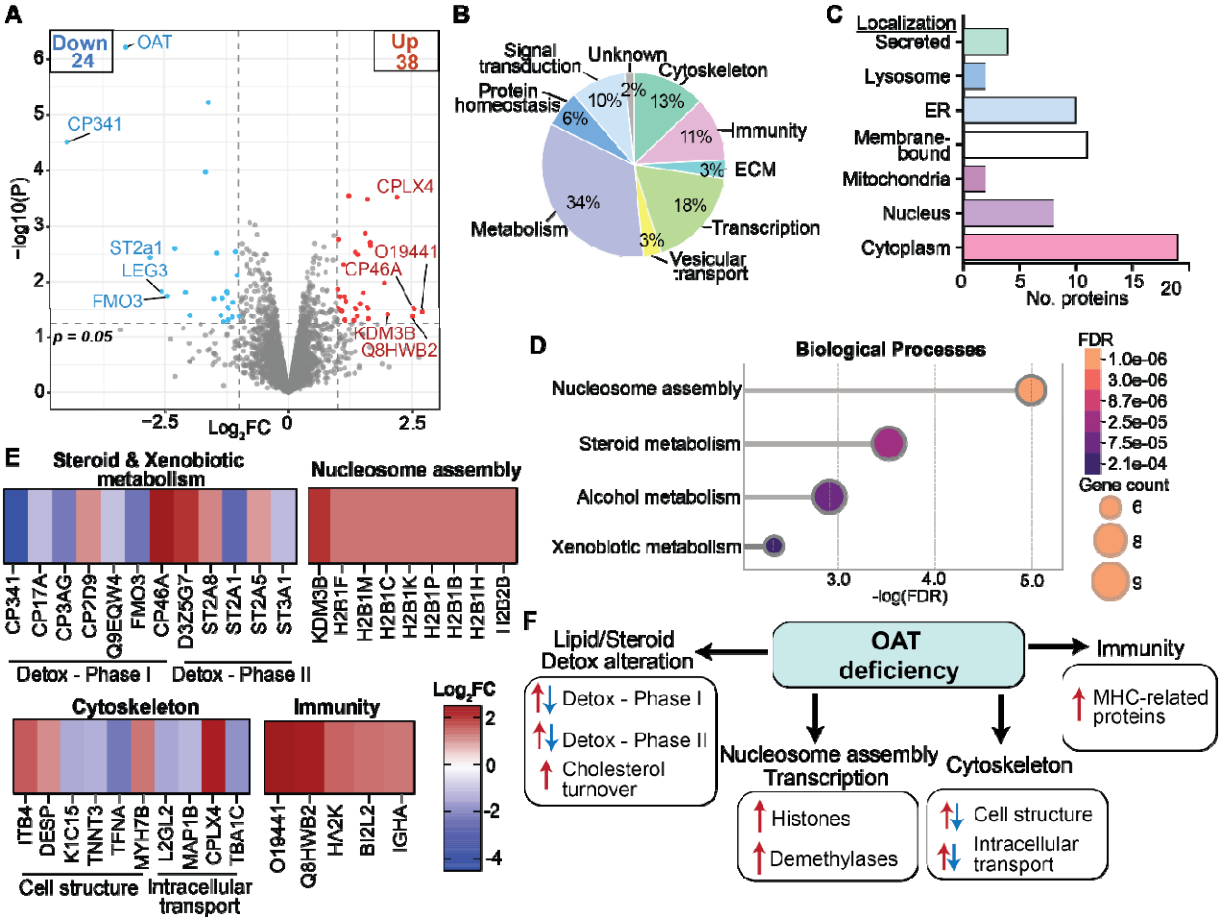

Figure 2. Proteomic changes in *Oat*^{rhg} adult liver. (A) Volcano plot showing top 5 DE proteins in proteomics data from *Oat*^{rhg} adult liver. **(B)** Functional classification of liver-enriched pathways based on manual curation using UniProt for protein function and NCBI literature search. **(C)** Categorized DE liver proteins by subcellular localization from UniProt annotations. **(D)** Top four enriched biological pathways in adult liver identified from the analysis of significantly DE proteins using STRING. **(E)** Heatmaps displaying an extended analysis of enriched pathways and their associated proteins with Log_2FC. **(F)** Schematic illustrating the key changes in *Oat*^{rhg} adults liver resulting from OAT deficiency. The upward red arrows and the downward blue arrows indicate the increased and decreased protein expression, respectively, for corresponding pathways. Detox – Phase I (oxidation/reduction by cytochrome P450 enzymes); Detox – Phase II (conjugation reactions such as sulfation and ester hydrolysis); Major Histocompatibility Complex (MHC); Endoplasmic reticulum (ER); Protein homeostasis (synthesis, degradation, folding, modifications). $1 \leq Log_2FC \leq -1$, p-value < 0.05.

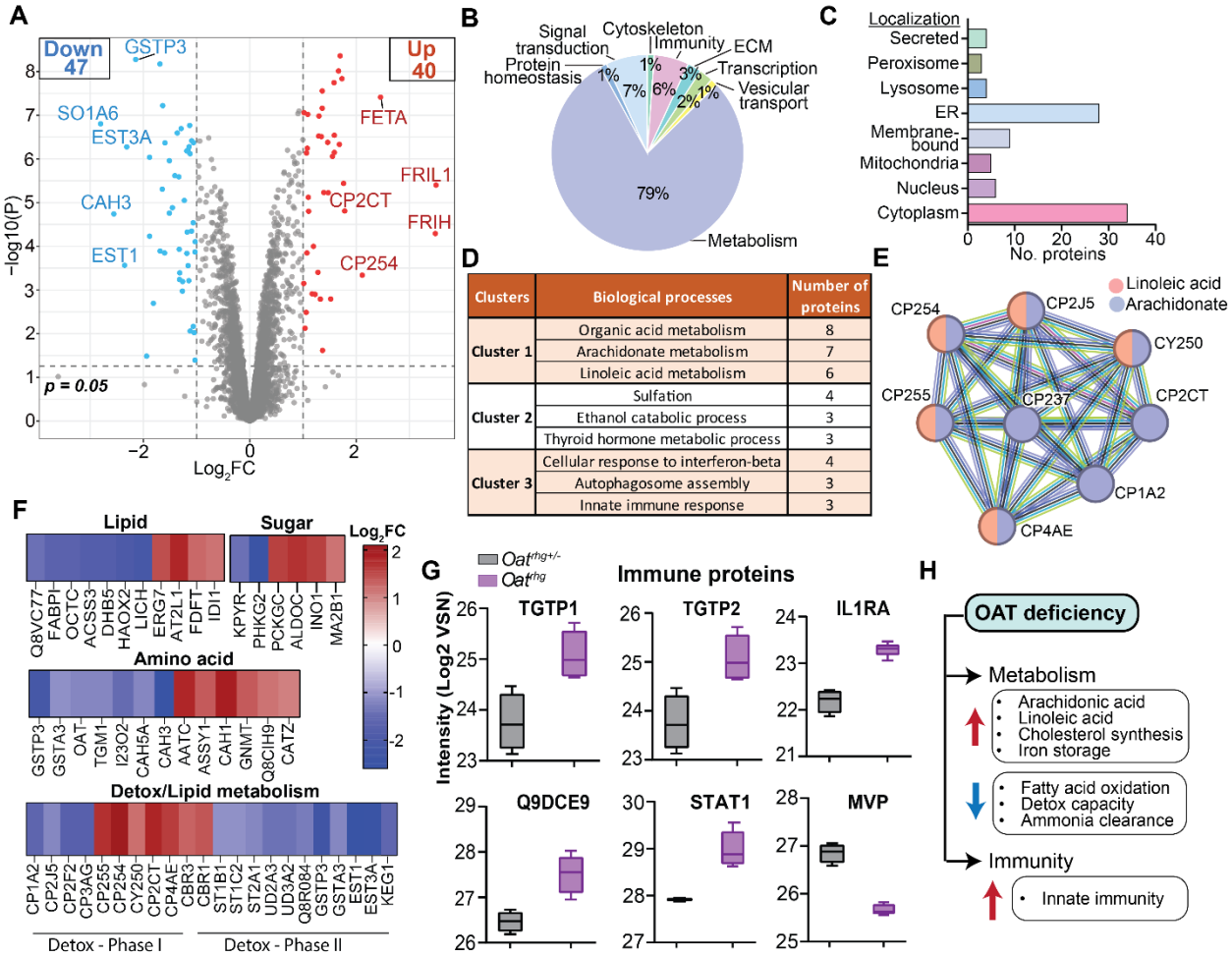

Figure 3. Proteomic changes in *Oat*^{rhg} neonate liver. (A) Volcano plot showing top 5 DE proteins in *Oat*^{rhg} neonates. **(B)** Liver-enriched pathways by functional classification through manual curation. **(C)** Categorized DE liver proteins by subcellular localization based on UniProt annotations. **(D)** Clusters of enriched biological processes identified using DAVID tool (FDR < 0.05). **(E)** The protein-protein interaction network for cluster 1 proteins based on STRING analysis. Nodes represent proteins and edges represent predicted functional associations. Edges are drawn in different colors to indicate distinct evidence sources used to support each interaction (Interaction score ≥ 0.4). **(F)** Heatmap of enriched metabolic proteins categorized into metabolic pathways, based on Log_2FC values. **(G)** The enriched immune-related proteins in liver *Oat*^{rhg} compared to *Oat*$^{rhg+/-}$. **(H)** Schematic summarizing the main changes in OAT-deficient neonatal liver. The upward red arrows and the downward blue arrows indicate the increased and decreased protein expression, respectively. Extracellular matrix (ECM); Endoplasmic reticulum (ER); Cytochromes P450 (CP, CY); Protein homeostasis (synthesis, degradation, folding, modifications). $1 \leq Log_2FC \leq -1$, p-value < 0.05.

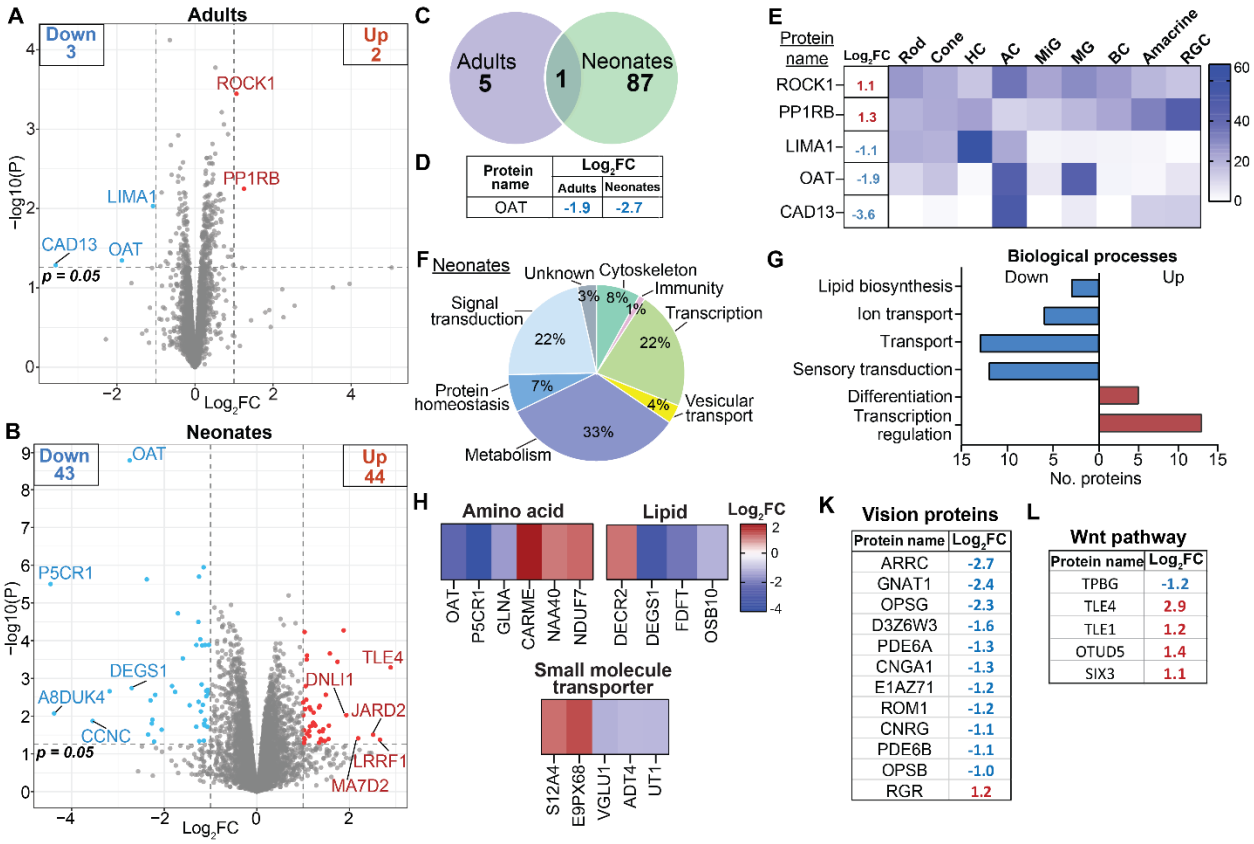

Figure 4. Proteomic changes in neonatal and adult Oat^{rhg} retinas. (A) Volcano plot showing top 5 DE proteins in *Oat^{rhg}* adults and **(B)** neonates. **(C-D)** Venn diagram and table showing unique and overlapping DE proteins in *Oat^{rhg}* adults and neonates. (**E**) Heatmap of DE proteins in *Oat^{rhg}* adults retina and their expression among retinal cell types based on mouse retina single cell sequencing data[33]. (**F**) Biological pathways enriched in *Oat^{rhg}* neonatal retina. **(G)** Bar chart showing enriched biological processes in neonates retina based on DAVID analysis. **(H)** Heatmaps showing DE metabolic proteins with Log_2FC in *Oat^{rhg}* neonates retina categorized in metabolic processes. **(K)** DE proteins related to vision and **(L)** Wnt pathway in the retina. Blue and red text denote down- and upregulated proteins in *Oat^{rhg}*, respectively. Horizontal cells (HC); Astrocytes (AC); Microglia (MiG); Müller glia (MG); ON and OFF Bipolar cells (BC); Retinal ganglion cells (RGC). $1 \leq Log_2FC \leq -1$, p-value < 0.05.

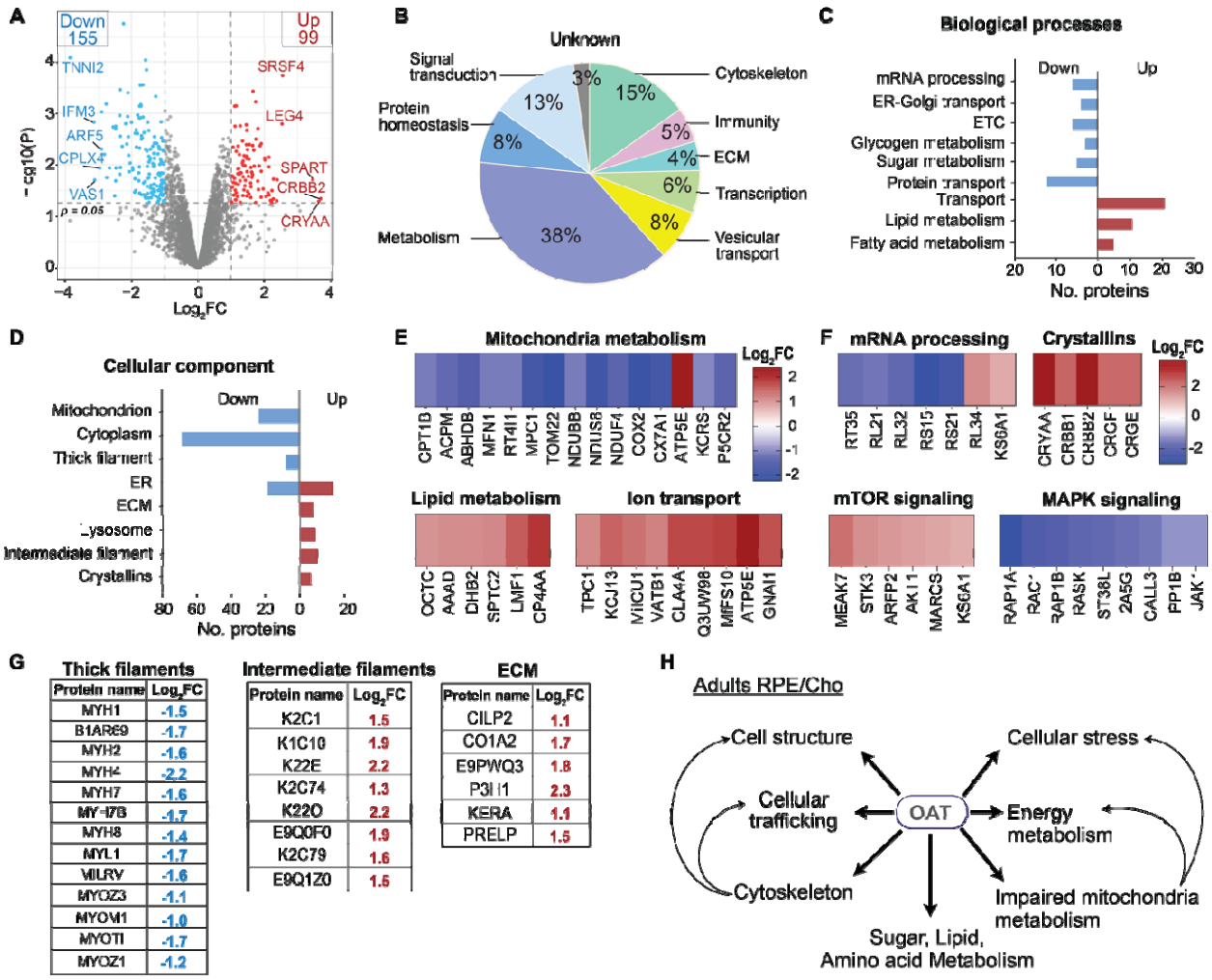

Figure 5. Proteomic changes in adult *Oat*^{rhg} RPE/Cho. (A) Volcano plot showing top 5 DE proteins in *Oat*^{rhg} adults RPE/Cho. **(B)** Pie chart shows enriched biological processes in *Oat*^{rhg} adults RPE/Cho. **(C)** GO analysis and **(D)** enriched cellular components for DE proteins in adult *Oat*^{rhg} RPE/Cho. Functional annotation was performed using DAVID. **(E-F)** Heatmaps showing significantly changed proteins and their Log_2FC grouped by enriched biological processes. **(G)** List of DE proteins in *Oat*^{rhg} associated with thick filaments (myosins), intermediate filaments (keratins), and extracellular matrix (ECM), with Log_2FC values. Red and blue indicate upregulated and downregulated proteins, respectively. **(H)** Schematic summary of key changes identified in adult RPE/Cho proteomics of OAT-deficient mice and their potential downstream effects. Endoplasmic reticulum (ER); Electron transport chain (ETC); the mammalian target of rapamycin (mTOR); mitogen-activated protein kinase (MAPK). $1 \leq Log_2FC \leq -1$, p-value < 0.05.

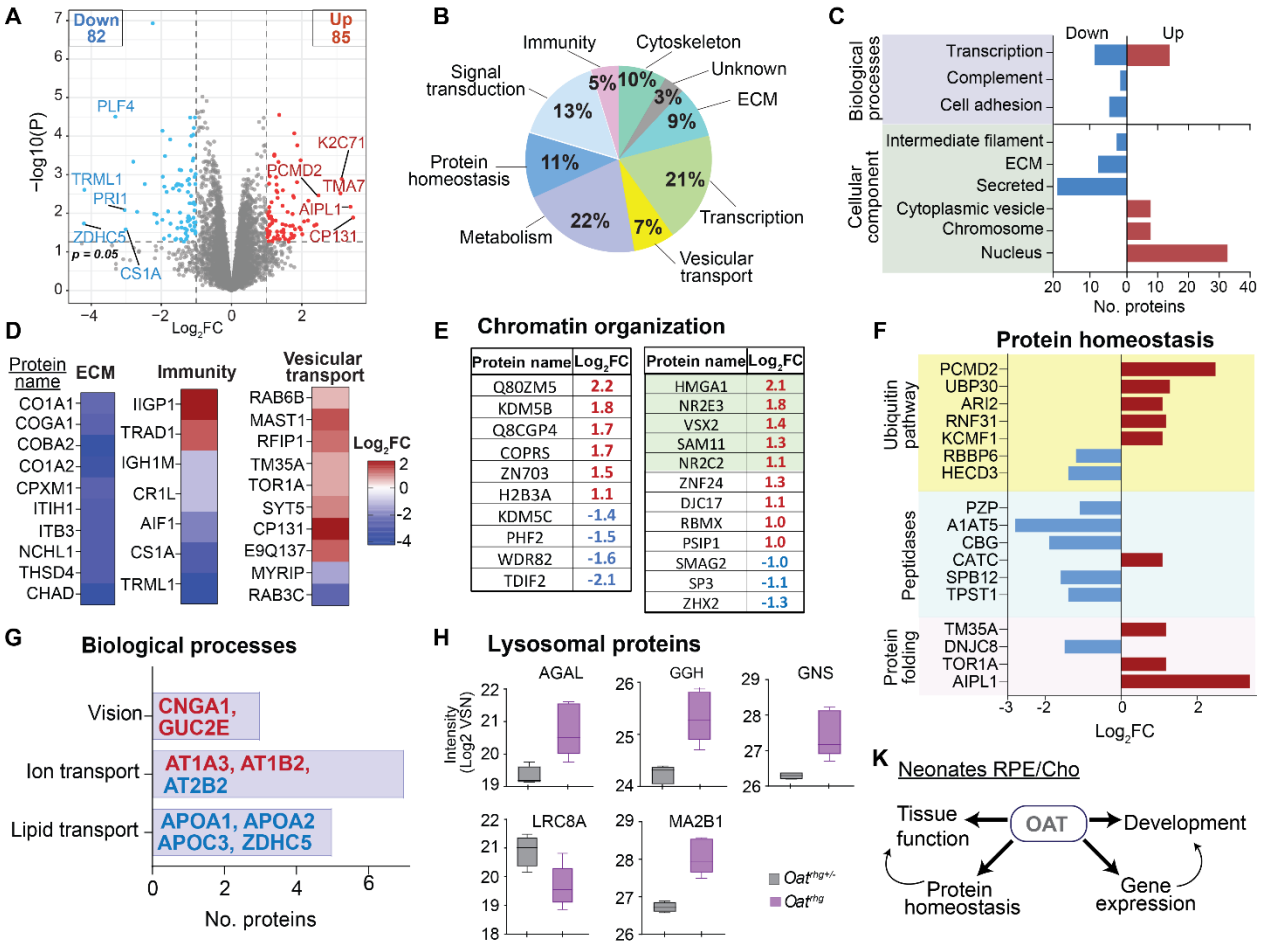

Figure 6. Proteomic changes in neonatal *Oat*^{rhg} RPE/Cho. (A) Volcano plot showing top 5 DE proteins in *Oat*^{rhg} neonates RPE/Cho. **(B)** Enriched biological processes in the RPE/Cho of *Oat*^{rhg}. **(C)** Enriched GO biological processes and cellular components based on DAVID functional annotation, with red and blue bars indicating up- and down-regulated processes, respectively. **(D)** Heatmaps showing enriched proteins associated with extracellular matrix (ECM), immune-related functions, and vesicular transport, with their Log_2FC expressions. **(E)** Significantly changed nuclear-related proteins in *Oat*^{rhg}, with light green highlighting those linked to retina and RPE/Cho development based on NCBI literature search. Blue and red texts denote down- and up-regulated proteins, respectively. **(F)** Bar chart showing DE proteins associated with protein homeostasis, grouped into ubiquitin pathway components, peptidases, and protein-folding regulators, with red and blue bars indicating up- and down-regulated, respectively, based on Log_2FC values. **(G)** Enriched biological pathways from the analysis of DE metabolic proteins in the neonate RPE/Cho. Up-regulated proteins are labeled in red and down-regulated in blue. **(H)** Bar graphs display DE lysosomal proteins based on UniProt function and subcellular

localization annotations. **(K)** Schematic summarizing proteomics changes in the RPE/Cho of OAT-deficient neonates. Extracellular matrix (ECM). $1 \leq Log_2FC \leq -1$, p-value < 0.05.

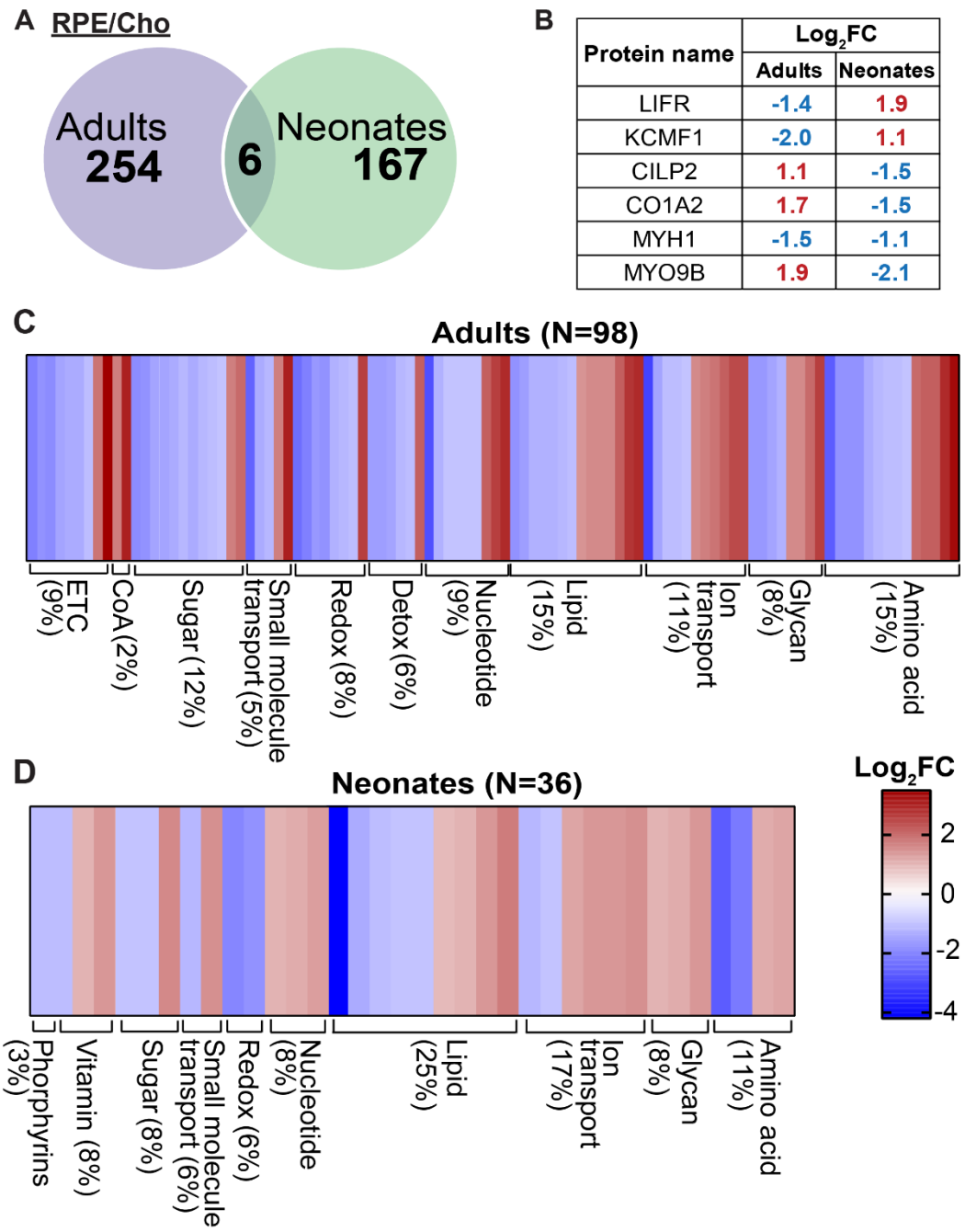

Protein name	Log$_2$FC	
	Adults	Neonates
LIFR	-1.4	1.9
KCMF1	-2.0	1.1
CILP2	1.1	-1.5
CO1A2	1.7	-1.5
MYH1	-1.5	-1.1
MYO9B	1.9	-2.1

Figure 7. Comparison of enriched proteomic profiles in RPE/Cho adults and neonates. **(A)** Total significantly changed and overlapping proteins in adults and neonates RPE/Cho. **(B)** Overlapping DE proteins between *Oat*^{rhg} adults and neonates. **(C)** Heatmap of enriched proteins clustered based on metabolic pathways for adults and **(D)** neonates with N showing the number of metabolic proteins enriched in each age group. Electron transport chain (ETC). $1 \leq \text{Log}_2\text{FC} \leq -1$, p-value < 0.05.

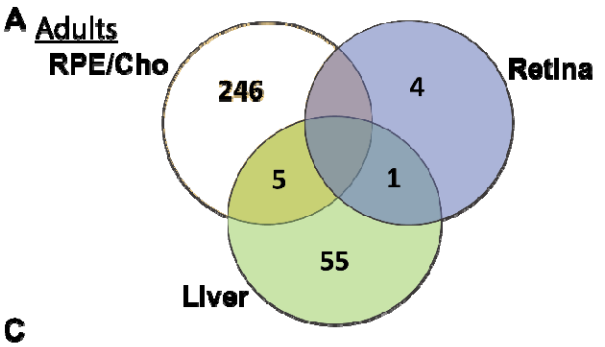

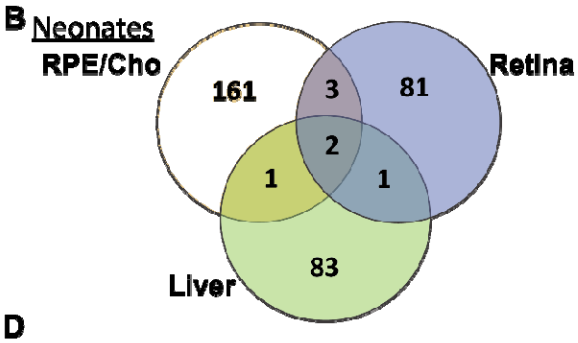

C

Protein ID	Log_2FC		
	RPE/Cho	Retina	Liver
OAT	-1.70	-1.87	-4.45
TNNT3	-1.07		-1.24
MYH7B	-1.68		1.37
CP341	-1.23		-4.47
CPLX4	-2.97		2.21
BGAL	1.39		1.13
Q8HWB2	1.60		3.41

D

Protein ID	Log_2FC		
	RPE/Cho	Retina	Liver
FETA	1.87	1.58	2.46
OAT	-2.25	-2.75	-1.16
MYRIP	-1.43	-1.07	
SP3	-1.07	1.42	
CNGA1	1.60	-1.26	
MA2B1	1.22		1.09
FDFT		-2.06	1.20

Figure 8. Cross-tissue proteomic overview of DE proteins in *Oat*^{rhg} adults and neonates. **(A)** The overlapped DE proteins in *Oat*^{rhg} in the RPE/Cho, retina, and liver for adults and **(B)** neonates. **(C)** Overlapping DE proteins in three analyzed tissues with the corresponding Log_2FC, in blue for downregulated, red for upregulated, black for non-significantly changed in *Oat*^{rhg} adults and **(D)** neonates, respectively. $1 \leq Log_2FC \leq -1$, p-value < 0.05.